ACOUSTIC PROPERTIES OF SANDSTONE

By

KHALID LOUDIYI

Bachelor of Science

Southwest Missouri State University

Springfield, Missouri

1980

Submitted to the Faculty of the Graduate College
of the Oklahoma State University
in partial fulfillment of the requirements
for the Degree of
MASTER OF SCIENCE
May, 1983

Thesis
1983
L886a
copy 2

OKLAHOMA STATE UNIVERSITY LIBRARY

ACOUSTIC PROPERTIES OF SANDSTONE

Thesis Approved:

James Lange
Thesis Adviser

Brian J Anderson

Norman N. Durham
Dean of the Graduate College

1153242

ACKNOWLEDGMENTS

The author would like to express his gratitude to the following for their assistance in the preparation of this master's thesis: Dr. James Lange, whose service in an advisory capacity helped to make this project possible; Mr. Heinz Hall, for his skill and expertise in the fashioning of the experimental apparatus used in this project; Dr. Geoff Summers and Dr. Bruce Ackerson for serving on this thesis advisory committee; Mr. Robert Quinn, for his grammatical assistance in the preparation of this thesis, and to Ms. Janet Sallee for her excellence in typing this thesis.

TABLE OF CONTENTS

Chapter		Page
I.	INTRODUCTION.	1
	Scope of Study	1
	Review of Literature	5
II.	EXPERIMENTAL PROCEDURE.	9
	Origin of the Rock Samples	9
	Basic Equipment.	9
	Porosity Measurement	14
	Velocity Measurement	15
III.	THEORETICAL BACKGROUND.	21
	Reflection and Transmission Phenomena.	21
	Shear and Compressional Wave Velocities in Fluid Saturated Porous Solids.	28
IV.	RESULTS AND DISCUSSION.	35
	Physical Characteristics of the Sandstone Samples. .	35
	Preliminary Results.	41
	Velocity-Time Dependence	44
	Velocity-Frequency Dependence.	48
	Pressure-Velocity Dependence	53
V.	SUMMARY AND FUTURE SUGGESTIONS.	68
BIBLIOGRAPHY.		70

LIST OF TABLES

Table		Page
I.	The Percentage Abundance of Sandstone Elements.	39
II.	Clays in the Sandstone Samples.	40
III.	Analysis of the Change in Velocity With Increasing Pressure for Water Saturated Sandstones.	60

LIST OF FIGURES

Figure		Page
1.	Illustration of Formations Associated With Trapping Hydrocarbons.	3
2.	Wave Velocity Versus Hydrostatic Pressure for Boise Sandstone.	7
3.	Location of the Experimental Samples From Noble County, Oklahoma	10
4.	Experimental Apparatus	11
5.	Pressure Apparatus	13
6.	Measurement of the Time of Flight of the Received Signal .	17
7.	Illustration of the Transmission and Reflection of Incident Wavefront From Media of Different Acoustic Impedances	18
8.	Change of Transmission Coefficient With Frequency.	29
9.	Histograms for the Sand Grains' Distribution of the Experimental Samples.	36
10.	Compressional Velocity Versus Porosity for the Sandstone Samples.	37
11.	Time of Flight of a Seismic Pulse in Water Versus Distance	42
12.	Change of P-Wave Group Velocity With Time for Sandstone Sample 1	45
13.	Change of P-Wave Group Velocity With Time for Sandstone Sample 4	46
14.	Change of P-Wave Group Velocity With Time for Sandstone Sample 5	47
15.	Change of Velocity With Frequency for Sandstone Sample 1 .	49
16.	Change of Velocity With Frequency for Sandstone Sample 2 .	50

Figure Page

17. Change of Velocity With Frequency for Sandstone Sample 4. . 51

18. Change of Velocity With Frequency for the Mesa Sandstone. . 52

19. Velocity Versus Applied Stress for Sandstone Sample 1 . . . 55

20. Velocity Versus Applied Stress for Sandstone Sample 2 . . . 56

21. Velocity Versus Pressure for Sandstone Sample 4 57

22. Velocity Versus Applied Stress for the Cockran Sandstone. . 58

23. Velocity Versus Pressure for the Mesa Sandstone 59

24. The Effect of Microcracks on the Velocity Parallel to the Direction of the Applied Stress for Sandstone Sample 1. . 62

25. The Effect of Microcracks on the Velocity Perpendicular to the Direction of Applied Stress for Sandstone Sample 1. . 63

26. The Effect of Cracks on the Velocity in the Direction of the Applied Stress for the Mesa Sandstone 65

27. Velocity Versus Applied Stress for the Mesa Sandstone Sample, the Applied Stress is Parallel to the Bedding Planes 66

CHAPTER I

INTRODUCTION

Scope of Study

The study of the earth's materials by means of their physical properties with appropriate instruments is the field of geophysics. The ever-increasing necessity for natural resources (oil, gas, water and minerals), has created a growing interest in this field, which in turn has led to great improvements in both the theory and technology used in the exploration and application of geophysics.

Geophysical prospecting for oil and gas is only about half a century old and its first contribution to oil discovery was in 1924 (2).

The scarceness of oil and gas, at shallow depths of the earth, led to the necessity of drilling and looking for these natural resources at thousands of feet below the earth's surface. The geophysical techniques used for this exploration are: seismic, gravitational, magnetic, electrical, electromagnetic, radioactivity, and well logging.

The method most widely used, for oil and gas explorations, is the seismic reflection method. This is mostly due to the ability of this method to penetrate deeply into the earth's sublayers and to the high resolution and accuracy it provides.

Briefly, the seismic reflection method maps the subsurface formations by using the time required for a seismic pulse to return to the

surface (or receivers), after reflections from interfaces having different acoustic impedances. The acoustic impedance is the product of the subsurface density and the wave's velocity. The seismic pulse is generated by means of a near-surface explosion or a nearby sound source (dynamite, mechanical impact, or vibration). The reflected pulses are recorded by a variety of detector arrays in response to the ground motion. The recorded data is stored on magnetic tape, so that computer processing can be used to enhance the signals with respect to the noise, extract the significant information, and display the data in such a form that a geological interpretation can be carried out readily. From the reflected data, the depths to reflecting interfaces can be obtained by analyzing the variation in reflection times and velocity information. Also, the attenuation and velocity characteristics can be used for identifying lithology. Thus, with the reflected data, it is possible to locate formations associated with the presence of oil and gas, such as anticlines, faults, salt domes, and reefs. Figure 1 gives a graphic illustration of such formations (11).

In order to extract more information from the reflected data, laboratory measurements are made on rock samples under conditions representing as closely as possible those occurring in the rock naturally. These measurements have revealed that seismic velocities in rocks are dependent on porosity (the volume of fluid enclosed in the sample by the volume of the sample), lithology, overburden and pore fluid pressure, temperature, nature and amount of pore fluids, intergranular elastic behavior, and microcracks.

The scope of this thesis is to investigate experimentally some of the acoustic properties of sandstone. Sandstone is one of the most

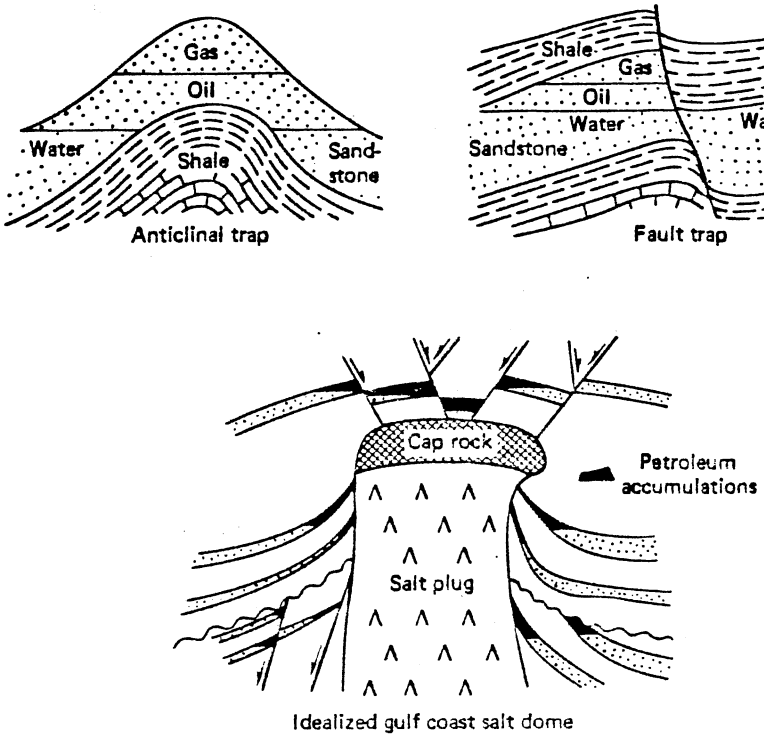

Source: E. A. Robinson and S. Treitel, Geophysical Signal Analysis (New Jersy, 1980), pp. 3.

Figure 1. Illustration Of Formations Associated With Trapping Hydrocarbons

familiar sedimentary rocks. It can be composed of many materials, but quartz grains are usually most abundant. The particles of sand in most sandstones are cemented by calcite, silica, or iron oxide. As with any sedimentary rock, sandstone can be characterized by its solid elastic matrix, randomly distributed pores, and saturating fluid. From these facts, one can conclude that the major factors that influence the velocities and attenuation in sandstone are, the degree of anisotropy of the solid matrix, the materials comprising the rock, the type of fluid saturating the pore spaces, and the effects of overburden and pore fluid pressure on the rock matrix.

The experimental set-up for this thesis is designed to apply only uniaxial confining (or overburden) stress on the sample (the effect of pore fluid pressure is not investigated here). The uniaxial stress, can be applied to the rock samples either in a direction perpendicular to or parallel to the decomposite layers (bedding planes). The velocity measurements are found by measuring the time it takes a seismic pulse to traverse the sample, both in the direction of the applied stress and perpendicular to this direction. This is done by placing ceramic piezoelectric crystals paralleled and perpendicular to the sample's bedding planes. The reason these measurements are made is to investigate the degree of velocity anisotropy in the samples and to determine how the uniaxial stress affects the velocity. The term velocity in this experiment refers only to the dilatational group velocity. In general, when a plane wave is incident on a free surface, it gives rise to both a reflected dilatational wave (P-wave) and a reflected shear wave (S-wave), which are polarized in a plane containing the incident and reflected waves. Since S-waves are not transmitted in liquids, they are not

investigated in this thesis.

The velocity is investigated for two different frequencies (20k Hz and 200k Hz). The effect of microcracks on the velocity are looked at for two of the experimental samples. The porosity of each sample is calculated and the composites of each sandstone sample are analyzed with the electron microscope and X-ray diffraction.

Review of Literature

One of the most common assumption in the field of exploration geophysics is that the subsurfaces of interest consist of beds whose properties are independent of direction. However, the assumption that the media are isotropic is a poor one. McCollum and Snell (9) reported that measurements made on outcrops of the Loraine shale in Canada, gave compressional wave velocities (P-wave) in the direction of the bedding planes (horizontal direction), nearly 33 percent greater than those in the vertical direction (perpendicular to the bedding planes) (9). In 1955, using geophones in wells and shots at various distances from the wells, Uhrig and Van Melle (16) indicated that horizontal P-wave speeds were 15-20 percent higher than vertical P-wave speeds for finely stratified media. These investigations established that many rocks are anisotropic. Anisotropy can be caused by many sources. The most probable of these for normal earth sectioning is called transverse isotropy. Transverse isotropy assumes physical properties are the same in all planes perpendicular to the one axis of symmetry (9). Postma (10) showed that earth section consisting of alternating plane and homogeneous alternating layers will appear to a seismic pulse to be transversely isotropic, for wavelengths long compared to individual bed thicknesses.

The axis of symmetry is vertical. Other kinds of anisotropy are quasi-anisotropy, associated with stratification not necessarily fine compared to the wavelength and homogeneous anisotropy in each homogeneous rock (16). There is also fractures in large volumes of inherently isotropic rock, that will cause the overall structure to be anisotropic. Finally, unequal preloading in the three directions, caused by large applied stresses, will cause an inherently isotropic rock to respond anisotropically (17).

The influence of liquid saturation and confining pressure on dilatational-wave velocity in sedimentary rocks has been discussed and determined experimentally by a number of workers, such as Hicks and Berry (7), Willie and collaborates (21), and Toksoz and collaborates (15). These workers have found that an increase in hydrostatic confining pressure with constant pore pressure increases both, the dilatational and shear wave velocities. Their data for changes in pore pressure indicates the velocity of dilatational wave to be a function of the difference, $(P_l - P_f)$, between the hydrostatic confining pressure (P_l), and pore pressure (P_f). These results agree with Biot's detailed analysis of the propagation of elastic waves in liquid-saturated isotropic porous media, in low frequency range and in the high frequency range (1). Two main conclusions from Biot's analysis are: First, the shear-wave velocity in a liquid saturated porous material will always be less than in the dry material. Second, the dilatational wave velocity in a liquid saturated porous material will generally be higher than in the dry material, except for materials having very low bulk compressibilities. Figure 2 (8) shows P-wave and S-wave group velocities versus the change in confining pressure for Boise sandstone, both dry and

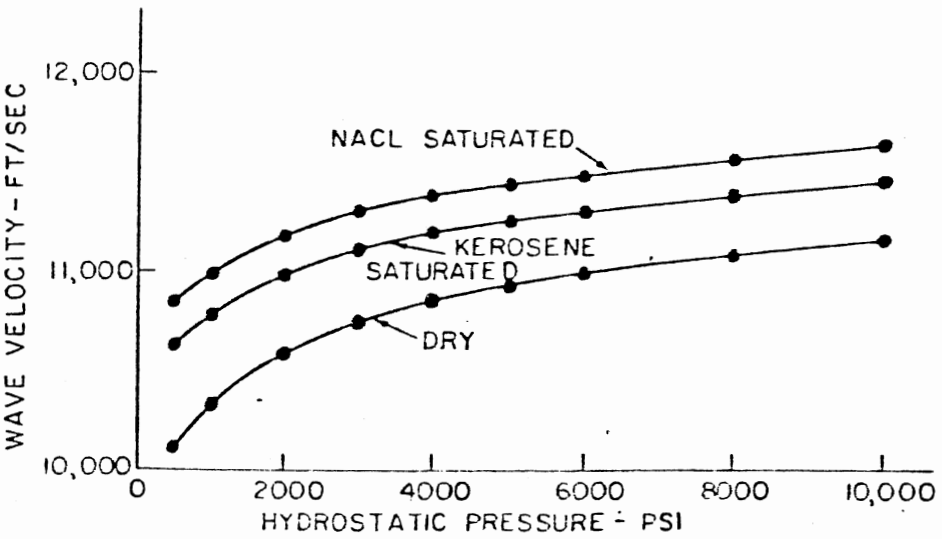

a.) Dilatational-Wave Group Velocities

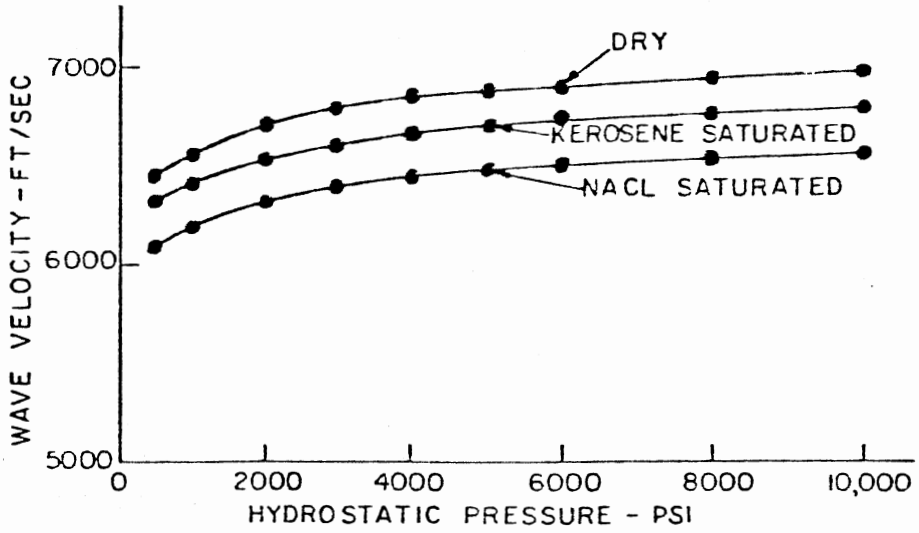

b.) Shear-Wave Group Velocities

Source: M. S. King, "Wave Velocities in Rocks as a Function of Changes in Overburden Pressure and Pore Fluid Saturants," Geophysics, XXXI (1966), pp. 50-73.

Figure 2. Wave Velocity Verses Hydrostatic Pressure For Boise Sandstone

saturated with NaCl and with kerosene. This figure shows that both the P-wave and S-wave velocities behavior are in agreement with the theory predicted by Biot.

Since sedimentary rocks may be partially saturated with one or more fluids, experimental data and theoretical models have been developed to see how does the partial saturation effect the compressional and shear velocities in sedimentary rocks. The important conclusion is that the undersaturation causes P-wave velocity to decrease more than the S-wave velocity, resulting in an observable decrease in the velocity ratio V_p/V_s. Incorporating such data with the "bright spots" leads to a good mean for detecting zones of gas saturation. Bright spots, or reflection amplitude anomalies, are a consequence of large seismic P-wave velocity and density (known as acoustic impedance) contrasts at boundaries of subsurface gas reservoirs caused by differences between the gas saturated reservoir rock and surrounding material.

CHAPTER II

EXPERIMENTAL PROCEDURE

Origin of the Rock Samples

Four of the sandstone samples used in this experiment were collected from Noble County, Oklahoma. These samples are labeled as sample #1, #2, #3, and #4. The approximate location of the area from which each sample was collected is shown in Figure 3 (12). According to Shelton (12), Sandstones from this area are part of the constituents of the Wellington formation, the lower most unit of the Cimarronian Series and of the Permian system. Such sandstones were characterized by Shelton (12) as being very fine grained, well to very well sorted, and quartz rich subarkoses.

The other two samples used in this experiment were cores from low permeability reservoirs. These cores were collected from the Department of Energy, at Bartlesville, Oklahoma. One of these samples came from a depth of 6088 ft. at Cockran No. 1 well, Pushmataha County, Oklahoma. The other sample came from a depth of 10570 ft. at No. 1 Mesa unit, Sublette County, Wyoming. The first sample will be referred to as the Cockran sample and the other as the Mesa sample.

Basic Equipment

The major experimental apparatus used for the velocity measurements is shown in Figure 4. It consists of a Shlumberger sweep generator, two

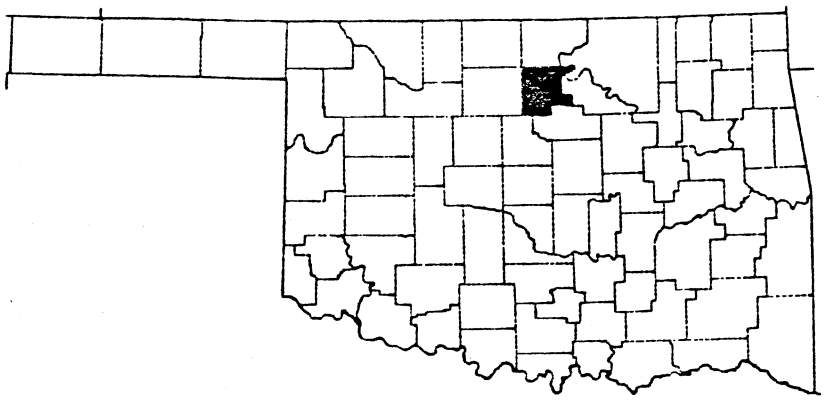

INDEX MAP OF OKLAHOMA SHOWING LOCATION OF NOBLE COUNTY

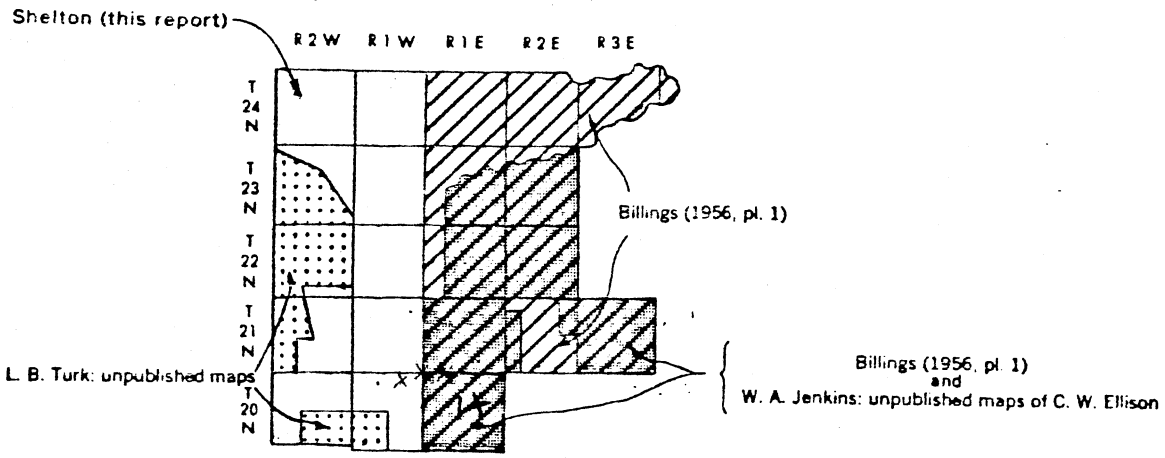

INDEX TO PRINCIPAL SOURCES OF GEOLOGIC MAPPING

Source: J. W. Shelton, R. H. Binaham and W. A. Jenkins, Geology and Mineral Resources of Noble County, Oklahoma, Oklahoma Geological Survey, Bulletin 128 (Norman, 1979).

Figure 3. Location Of The Experimental Samples From Noble County, Oklahoma

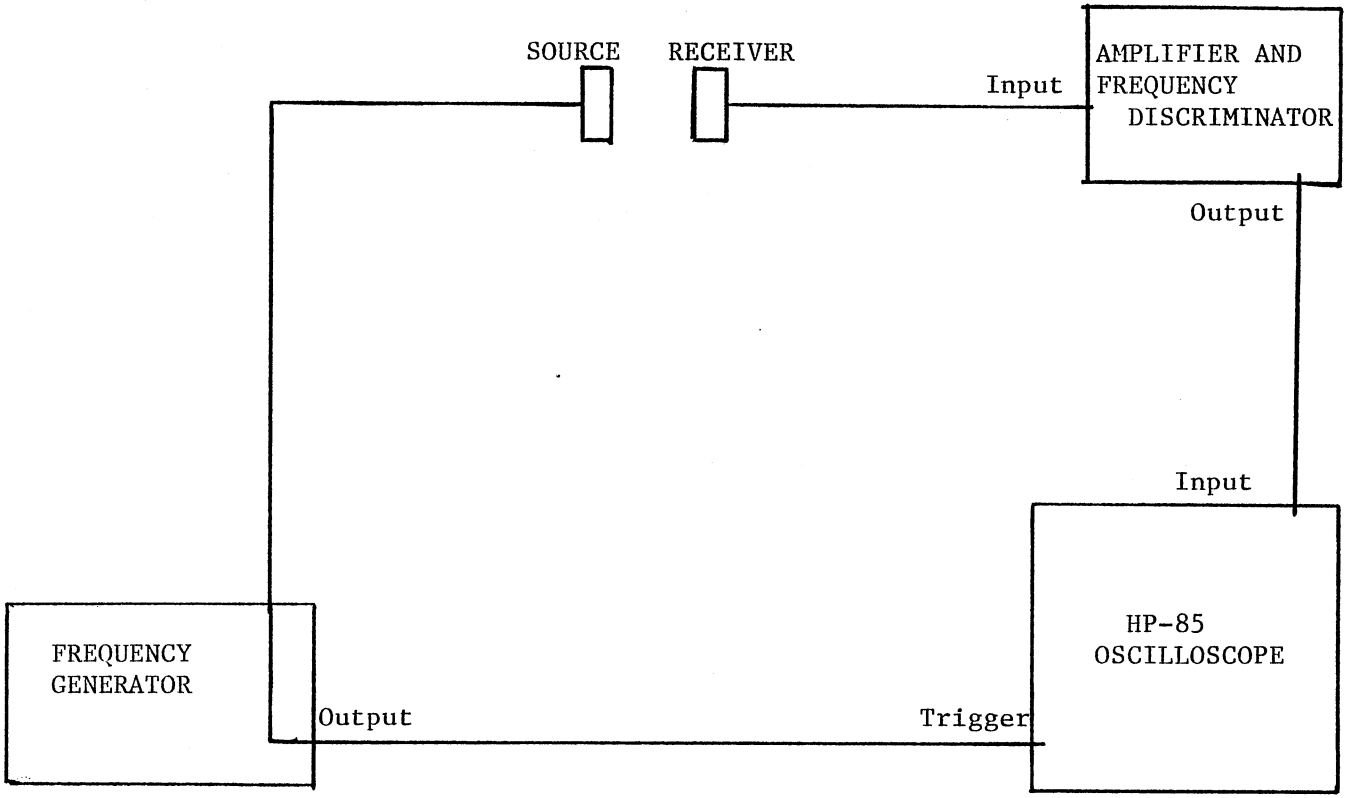

Fiugre 4. Experimental Apparatus

sets of hydrophones (transducers), a frequency descriminator, an amplifier, an oscilloscope, a pressure apparatus and a water tank.

The frequency generator is used to apply a sinusoidal voltage pulse to a transducer at its resonant frequencies, chosen to be 20k Hz and 200k Hz. The mechanical pulse produced by the transducer is transmitted through the saturating fluid (water in this experiment), the rock sample, and is then detected by a second transducer which is mounted at the other end of the sample. The set of transducers, source and receiver, are placed so that waves reflected or refracted by the tank boundaries, the water's surface, or the pressure apparatus' boundaries reach the receiver well after the direct wave. The electrical signal produced by the receiving transducer is amplified with a high gain differential amplifier. Meanwhile, a frequency descriminator is used to pick up those frequencies within the range of 10k - 30k Hz, or 10k - 300k Hz, depending on whether the source was resonating at 20k Hz, or 200k Hz. The amplified signal is displayed on the Hewell packet 1980-B oscilloscope. The oscilloscope's digital waveform storage function is then used to digitize and store the received signal at different amplifications. Finally the stored signals are recalled for time measurements of the pulse's duration from the source to the receiver.

The pressure apparatus is shown in Figure 5. It basically consists of an Enerpac hydraulic pump and cylinder. The hydraulic oil pump is hand operated and it can apply a pressure ranging from 0 - 10,000 psi to the hydraulic cylinder's ram. Connected to the end of this ram is an aluminum plate. Similarly, another plate of the same dimensions is placed at the lower part of the pressure apparatus. Each one of these plates has a hole drilled in its center. The dimensions of these holes

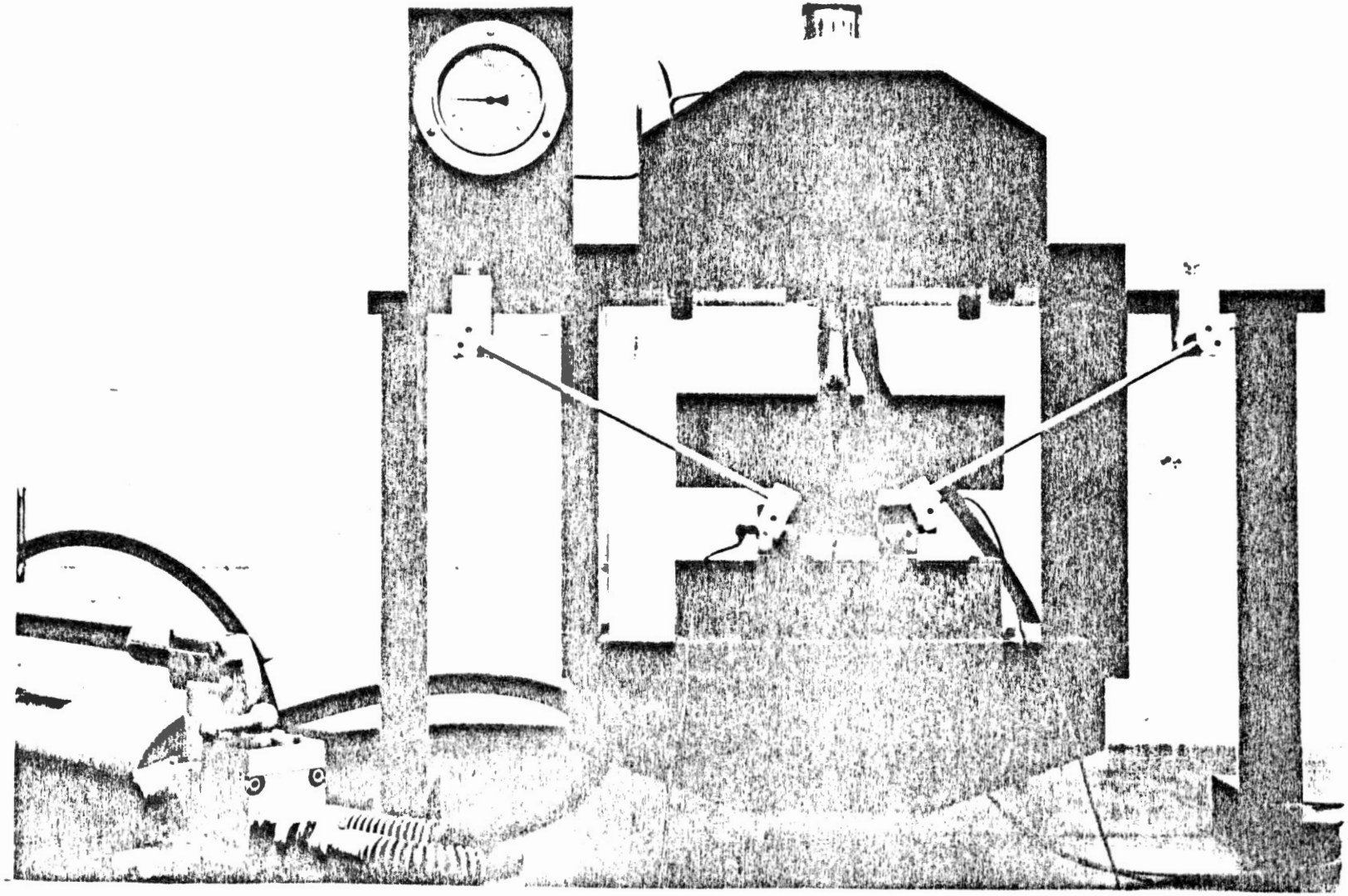

Figure 5. Pressure Apparatus

are large enough for placing the transducers (source and receiver) inside the plates. These transducers are kept in their position by using plastic holders to support them inside the hole, then each hole is covered with a stainless steel plate. These stainless steel plates have small holes drilled throughout to allow for the transmission of the seismic pulse's energy.

Porosity Measurement

The dependence of the measured velocity on the porosity is shown in the time average formula, as suggested by Wyllie et al. (18). This formula defines the intergranular porosity in terms of the total formation velocity, rock matrix velocity and fluid velocity. The relationship is expressed in the following equation:

$$\frac{1}{V_m} = \frac{\phi}{V_f} + \frac{1-\phi}{V_r} \qquad (2\text{-}1)$$

where V_m = measured velocity, V_f = velocity in saturating liquid, V_r = velocity in rock solid, and ϕ = volumetric porosity fraction. Also, since the porosity of a sample gives an idea of the available pores for enclosing either gas or oil, this makes porosity measurements very important in classifying the physical properties of different rock samples.

The porosity measurements carried in this lab are done by cutting sub-samples from the original sandstones. These samples are placed in a desiccator and left under an aspiration process for at least 24 hours. After taking each sample out of the desiccator, the excess water on its surface is dried with paper towels, and the saturated sample's weight

is recorded up to 1/10000 of a gram by using the 'Storius' pan scale. Afterwards, the samples are left at room temperature and atmospheric pressure for a few days, the weight and dimensions of the completely dry samples are recorded. The porosity of each sandstone sample is found by taking an average of its sub-samples' porosities. These are found by dividing the volume of pore spaces (V_p) by the sample's volume (V_s). Now, if all the pores were saturated with water, their volume can be found by using $V_p = \rho_\omega \cdot m_w$ where ρ_ω is the water density (1 gr/cm^3) and m_w is the mass of water occupying the pores. In terms of an equation the porosity is written as:

$$\phi = \frac{V_p}{V_s} = \frac{\rho_\omega \cdot m_w}{V_s}$$

$$\phi = \frac{m_w \cdot (1 \text{ gr/cm}^3)}{V_s}$$

But m_w = m(saturated sample) - m(dry sample), thus,

$$\phi = \frac{\text{m(saturated sample)} - \text{m(dry sample)}}{V_s} \cdot (1 \text{ gr/cm}^3) \qquad (2.2)$$

Velocity Measurement

Basically, there are three laboratory techniques suitable for measuring the dilatational wave velocities on rock samples subject to confining stress, these are: the resonance method, the rotating plate technique and the pulse first-arrival technique (8). In this experiment, the pulse first-arrival technique is used in measuring the time it takes a sinusoidal pulse to traverse a known thickness of a rock sample. Since

the oscilloscope is triggered at the start of the generated sine pulse's first cycle, the time it takes the pulse to traverse the distance from the source to the receiver is measured from this point to the beginning of the received pulse (as shown in Figure 6).

The transducers in the direction of the applied stress are not placed directly on the saturated sandstones, they are separated by water and stainless steel plates. However, the distance between the transducers and the sample is fixed. Thus, with the aluminum blocks bound together, a measurement is made to obtain the time taken for the seismic pulse to travel through the water and stainless steel plates. The rock sample is then placed between the two aluminum blocks, and a second measurement is made to obtain the time taken for a seismic pulse to travel through the water, stainless steel plates and the rock sample. Subtracting from the second time value (time taken for the pulse to traverse the stainless steel plates, water and rock sample), the first time value (time taken for the pulse to traverse the stainless steel plates and water), we obtain the time taken for the pulse to traverse the rock sample. Dividing this value by the measured thickness of the sandstone sample we obtain the velocity in the direction of the applied stress. Labeling this velocity by V_1, the thickness of the sample in the direction of the applied stress by D_1, and the first and second time values by t_1 and t_2, then V_1 can be written in terms of an equation as

$$V_1 = \frac{D_1}{t_2 - t_1} . \tag{2.3}$$

The velocity in the direction perpendicular to the applied stress is found by placing a second set of transducers between the two aluminum

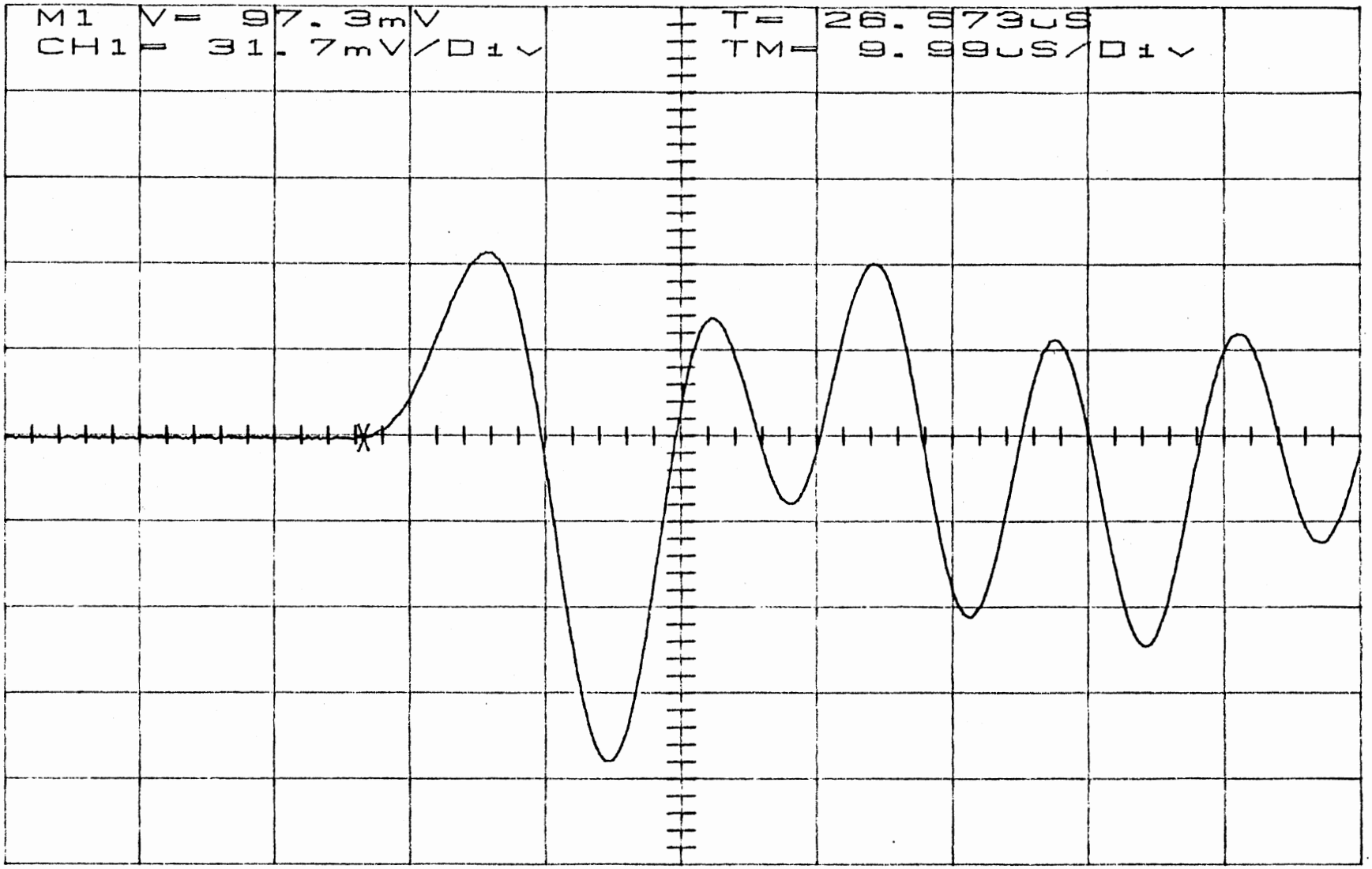

Figure 6. Measurement Of The Time Of Flight Of The Received Signal

blocks (see Figure 5). The transmitting and receiving transducers in this direction are moveable along a rail fixed to the pressure apparatus, and are submerged in the water tank. Due to practical experimental convenience, these hydrophones (transducers) are not connected directly to the sandstone samples. This means that the received pulse travels partially in the water and partially in the saturated sample. The time it takes a seismic pulse in water to traverse a distance D between the source and receiver (with no sample present) is $t_w = D/V_w$, where V_w is the velocity of a seismic pulse in water. If a sample of thickness D_2 ($D_2 < D$) is placed between the source and receiver there will be a distance D_w where the direct pulse travels in water. This is given by

$$D_w = D - D_2$$

In this case, the time (T) it takes the pulse to traverse the distance between the source and receiver is given by,

$$T = t_s + t_w$$

$$= \frac{D_2}{V_2} + \frac{D_w}{V_w} = \frac{D_2}{V_2} + \frac{D - D_2}{V_m}$$

$$= t_w + D_2\left(\frac{1}{V_2} - \frac{1}{V_w}\right)$$

or

$$V_2 = \left[\frac{T - t_w}{D_2} + \frac{1}{V_w}\right]^{-1} \qquad (2.4)$$

Thus by measuring t_w, T, D_2 and V_w we can use the last equation to find the sample's velocity in the direction perpendicular to the applied stress. This velocity is denoted by V_2.

CHAPTER III

THEORETICAL BACKGROUND

Reflection and Transmission Phenomena

When a wave front meets a boundary, it gives rise to reflected and transmitted waves. The nature of these waves depends on several factors including the properties of the incident wave, the angle of incidence, the nature of the boundary, and so forth.

The simplest case deals with plane waves at normal angles of incidence with the boundary. Considering the boundary to be an infinite plane, then this becomes a boundary value problem. At one side of the boundary there is an infinite half plane with acoustic impedance $\rho_1 c_1$, and on the other side another infinite half plane of acoustic impedance $\rho_2 c_2$. Taking the direction of incidence as the x-axis, the displacement on each side of the boundary can be written as,

$$U_1 = A_i \exp(i(kx - wt)) + A_r \exp(-i(kx = wt)), \qquad (3.1)$$

$$U_2 = A_t \exp(i(k'x - wt)) \qquad (3.2)$$

Where A_i, A_r and A_t correspond to the amplitudes of the incident, reflected, and transmitted waves (respectively), k and k' are the wave number in media 1 and 2 (respectively), and w is the angular velocity of the wave. At the boundary (x=0) the displacement and the normal component of stress are continuous. Applying from the first boundary

condition, the following equation is obtained,

$$U_1(x=0) = U_2(x=0)$$

or

$$A_i + A_r = A_t \tag{3.3}$$

From the continuity of the normal component of stress

$$\rho_1 c_1^2 [(\partial U_1)/(\partial x)]_{x=0} = \rho_2 c_2^2 [(\partial U_2/\partial x)]_{x=0}$$

we obtain,

$$\rho_1 c_1^2 (kA_i - kA_r) = r_2 c_2^2 k' A_t \tag{3.4}$$

Substituting the value of A_t from Equation (3.3) leads to,

$$\rho_1 c_1^2 \cdot (kA_i - kA_r) = \rho_2 c_2^2 k' (A_i + A_r)$$

$$A_r/A_i = (\rho_1 c_1^2 k - \rho_2 c_2^2 k')/(\rho_1 c_1^2 k + \rho_2 c_2^2 k')$$

but, $k = (w/V_1) = (w/c_1)$ and $k' = (w/c_2)$, then,

$$A_r/A_i = (\rho_1 c_1 - \rho_2 c_2)/(\rho_1 c_1 + \rho_2 c_2) \; . \tag{3.5}$$

This ratio describes the reflection coefficient, which is a measure of the reflected amplitude with respect to the incident amplitude, it is denoted by R, where

$$R = A_r/A_i \tag{3.6}$$

The transmission coefficient, T, describes the ratio between the transmitted amplitude and the incident amplitude:

$$T = A_t/A_i \tag{3.7}$$

The above ratio is found by solving for A_r in Equation (3.3) and substituting the result in Equation (3.4). Thus,

$$A_t/A_r = (2\rho_1 c_1)/(\rho_1 c_1 + \rho_2 c_2) \ . \tag{3.8}$$

Note that when $\rho_1 = \rho_2$ and $c_1 = c_2$, this leads to the trivial result of R=0 and T=1, which is in fact the expected result when the wave travels in the same medium. The same result is obtained if both media have the same acoustic impedance ($\rho_1 c_1 = \rho_2 c_2$). In this case the incident wave does not see the boundary and continues its path as if there was no change in the medium.

This sample analysis of the trivial case for the reflection and transmission phenomena can be made more challenging by adding more boundaries. The next case would be to introduce another infinite plane, a distance ℓ from the original infinite plane boundary as shown in Figure 7. This can be thought of as an infinite sample of thickness 1, and acoustic impedance $\rho_2 c_2$, immersed in a medium of acoustic impedance $\rho_1 c_1$. Only one dimensional plane waves at normal incidence with the boundary, will be considered here. Furthermore, the transient effects that may exist initially are not considered. That is, the assumption that the field is fully developed is made here. With these conditions, the displacement in the three media (shown in Figure 7) are given by:

$$U_1 = A_i \exp(i(kx - wt)) + A_r \exp(-i(kx + wt)) \tag{3.9}$$

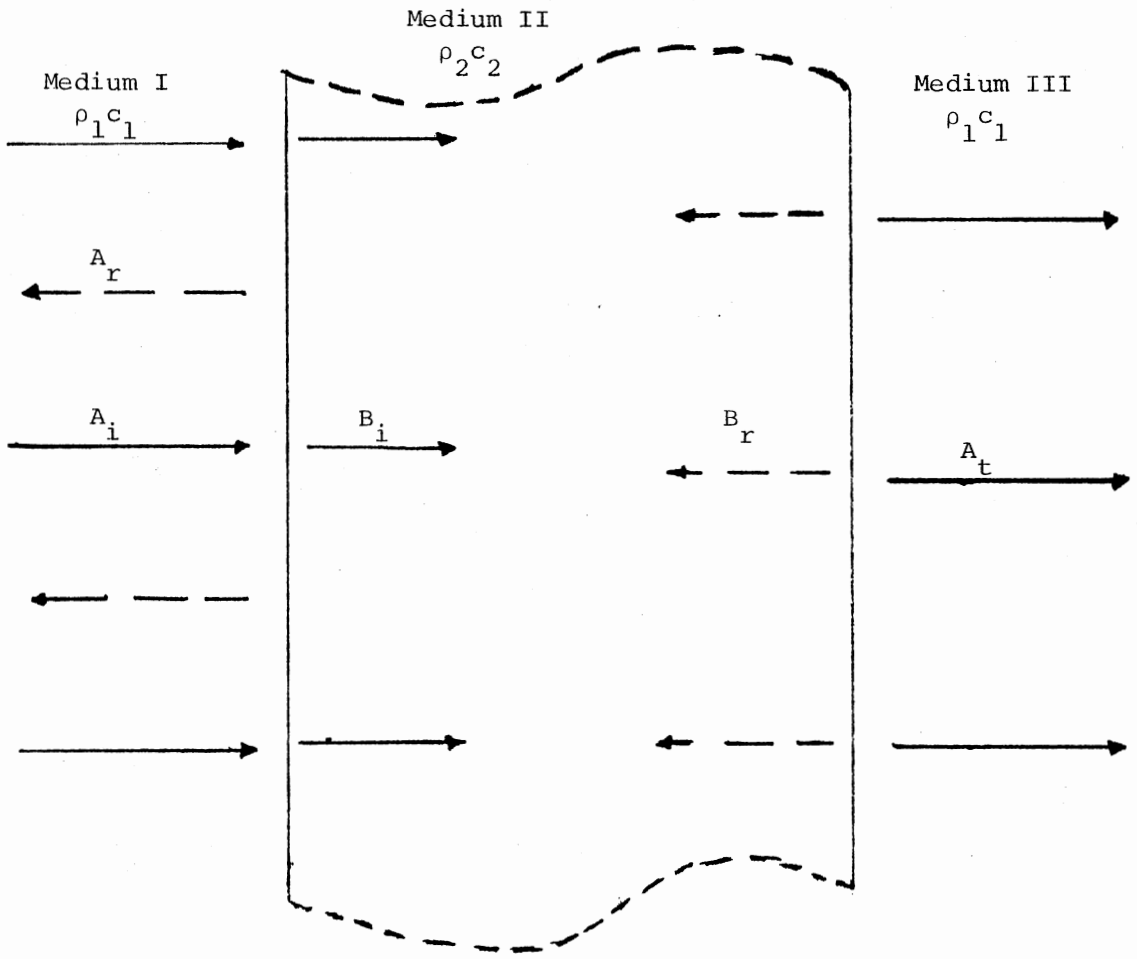

Figure 7. Transmission and Reflection From a Solid. Illustration of the Transmission and Reflection of Incident Wavefront From Media of Different Acoustic Impedances

$$U_2 = B_i \exp(i(k'x - wt)) + B_r \exp(-i(k'x + wt)) \tag{3.10}$$

$$U_3 = A_t \exp(i(kx - wt)) \tag{3.11}$$

Now applying the boundary conditions at x=0 and at x=1,

$$U_1(x=0) = U_2(x=0), \quad U_2(x=1) = U_3(x=1)$$

$$\rho_1 c_1^2 (\partial U_1)/(\partial x)\Big|_{x=0} = \rho_2 c_2^2 (\partial U_2)/(\partial x)\Big|_{x=0}$$

$$\rho_2 c_2^2 (\partial U_2)/(\partial x)\Big|_{x=1} = \rho_1 c_1^2 (\partial U_3)/(\partial x)\Big|_{x=1} .$$

After the appropriate substitutions, the following equations are obtained at the boundary x=0,

$$A_i + A_r = B_i + B_r \tag{3.12}$$

$$\rho_1 c_1^2 k \cdot (A_i - A_r) = \rho_2 c_2^2 k' \cdot (B_i - B_r) \tag{3.13}$$

and at x=a,

$$B_i \exp(ik'1) + B_r \exp(-ik'1) + A_t \exp(ik1) \tag{3.14}$$

$$\rho_2 c_2^2 k B_i (\exp(ik'1 - B_r \exp(-ik'1)) = \rho_1 c_1^2 k A_t \exp(ik1) . \tag{3.15}$$

These last four equations can be arranged in a matrix form such as,

$$\begin{pmatrix} -1 & 1 & 1 & 0 \\ \rho_1 c_1^2 k & \rho_2 c_2^2 k' & -\rho_2 c_2^2 k' & 0 \\ 0 & \exp(ik'l) & \exp(-ik'l) & -\exp(ikl) \\ 0 & \rho_2 c_2^2 k' \exp(ik'l) & -\rho_2 c_2^2 k' \exp(-ik'l) & -\rho_1 c_1^2 k \exp(ikl) \end{pmatrix} \cdot \begin{pmatrix} A_r \\ B_i \\ B_r \\ A_t \end{pmatrix} =$$

$$A_i \cdot \begin{pmatrix} 1 \\ \rho_1 c_1^2 k \\ 0 \\ 0 \end{pmatrix}$$

Letting "DET" be the determinant of the 4 by 4 matrix, and after the mathematical manipulations, it is found that,

$$DET = w^2 \exp(ikl) \cdot (4\rho_1 c_1 r_2 c_2 \cos(k'l) - 2i((\rho_1 c_1)^2 + (\rho_2 c_2)^2)\sin(k'l))$$

Solving for A_t it is found that,

$$A_t = \frac{\begin{vmatrix} -1 & 1 & 1 & 1 \\ \rho_1 c_1^2 k & \rho_2 c_2^2 k' & -\rho_2 c_2^2 k' & \rho_1 c_1^2 k \\ 0 & \exp(ik'l) & \exp(-ik'l) & 0 \\ 0 & \rho_2 c_2 k' \exp(-ik'l) & -\rho_2 c_2 k' \exp(-ik'l) & 0 \end{vmatrix} \cdot A_i}{DET}$$

$$A_t = \frac{2 \cdot \rho_1 c_1 \rho_2 c_2 \cdot A_i}{M} \tag{3.16}$$

where,

$$M = \exp(ikl) \cdot (2\rho_1 c_1 \rho_2 c_2 \cos(k'l) - i((\rho_1 c_1)^2 + (\rho_2 c_2)^2 \sin(k'l)) \ .$$

Similarly, the reflection amplitude is found to be:

$$A_r = \frac{i((\rho_2 c_2)^2 - (\rho_1 c_1)^2) \sin(k'l) \cdot A_i}{2 \cdot \rho_1 c_1 \rho_2 c_2 \cos(k'l) - i((\rho_1 c_1)^2 + (\rho_2 c_2)^2)^2 \sin^2(k'l)} \tag{3.17}$$

From Equations (3.16) and (3.17), it is apparent that both A_t and A_r have complex amplitudes; implying that the incident wave is not in phase with the transmitted and the reflected waves. Considering the ratio of transmitted to incident intensities (I_t/I_i),

$$\frac{I_r}{I_i} = \frac{A_t \cdot A_t^*}{A_i \cdot A_i^*} = \frac{4}{4\cos^2(k'l) + (\rho_2 c_2/\rho_2 c_2 + \rho_2 c_2/\rho_1 c_1)^2 \sin^2(k'l)} \cdot \tag{3.18}$$

Similarly, the ratio of reflected-to-incident intensities (I_r/I_i) is given by,

$$\frac{I_r}{I_i} = \frac{A_r \cdot A_r^*}{A_i \cdot A_i^*} = \frac{(\rho_2 c_2/\rho_1 c_1 - \rho_1 c_1/\rho_2 c_2)^2 \sin^2(k'l)}{4\cos^2(k'l) + (\rho_2 c_2/\rho_1 c_1 + \rho_1 c_1/\rho_2 c_2)^2 \sin^2(k'l)} \cdot \tag{3.19}$$

Note that when $\rho_1 = \rho_2$ and $c_1 = c_2$, this gives the trivial result of the energy's total transmission, $I_t/I_i = 1$ and $I_r/I_i = 0$. Also, in the case of $\rho_1 c_1 = \rho_2 c_2$, the whole energy is transmitted. In this case the three regions have the same acoustic impedances, and the incident

wave continues its path as if the material of thickness 1 was transparent to it. When $\rho_2 c_2 >> \rho_1 c_1$, Equations (3.18) and (3.19) reduce to,

$$\frac{I_t}{I_i} = \frac{4}{4\cos^2(k'1) + (\rho_2 c_2/\rho_1 c_1)^2 \sin^2(k'1)}$$

and

$$\frac{I_r}{I_i} = \frac{(\rho_2 c_2/2\cdot\rho_1 c_1)^2 \sin^2(k'1)}{\cos^2(k'1) + (\rho_2 c_2/2\cdot\rho_1 c_1)^2 \sin^2(k'1)}$$

This case is similar to having air in media, 1 and 3 and a dense solid in medium 2.

From Equations (3.18) and (3.19), it is seen that the transmission coefficient and reflection coefficient are strongly dependent on k'1 ($w1/c^2$). More specifically, if we have a material of a given thickness 1 and compressional acoustic velocity c_2, then (I_t/I_i) and (I_r/I_i) become very strongly dependent on the frequency. We also see that there are many frequencies for which $(I_t/I_i) = 1$ and $(I_r/I_i) = 0$. These frequencies are found by setting,

$$\sin(k'1) = 0$$

which leads to,

$$k'1 = \frac{w1}{c_2} = n\pi \quad \text{where } n = 0, 1, 2, \ldots$$

Such frequencies correspond to the characteristic frequencies of the region $0 \leq x \leq 1$. So, if the incoming wave has a frequency that

matches one of these characteristic frequencies then we get resonance. This resonance causes the sample to act as a perfect transmitter.

The change of I_t/I_i with wl/c_2 is shown in Figure 8 for different values of characteristic impedances ratio. This figure demonstrates, for a given value of l and c_2, the effects of frequency on transmission. We see that for most frequencies, the sample acts as an effective barrier for seismic wavefronts, except in the range of resonant frequencies, where the transmitted energy approaches the incident energy's amplitude. The same figure, also, demonstrates that the larger the difference between the two characteristic impedances, the smaller the E_t/E_i gets.

Shear and Compressional Wave Velocities in Fluid Saturated Porous Solids

The purpose of this section is to give a general background to the derivation of elastic wave velocities in porous elastic solids saturated by a viscous fluid.

Biot (1) gave a general theory for a three-dimensional propagation of elastic waves in a fluid saturated porous solid. Since the development of this theory, it has been known that in such a system (fluid-solid system), provided both solid and fluid consist of continium, two entirely different, coupled, dilatational waves and shear waves are generated as a sound source (4).

According to Biot (1), the basic equations describing such dilatational waves in a fluid saturated solid are,

$$\nabla_1^2\{(P+S)e + Q\varepsilon\} = \frac{\partial^2}{\partial t^2}(\rho_{11}e + \rho_{12}\varepsilon) + \frac{\mu\phi^2}{k}\frac{\partial}{\partial t}(e-\varepsilon) \qquad (3.20)$$

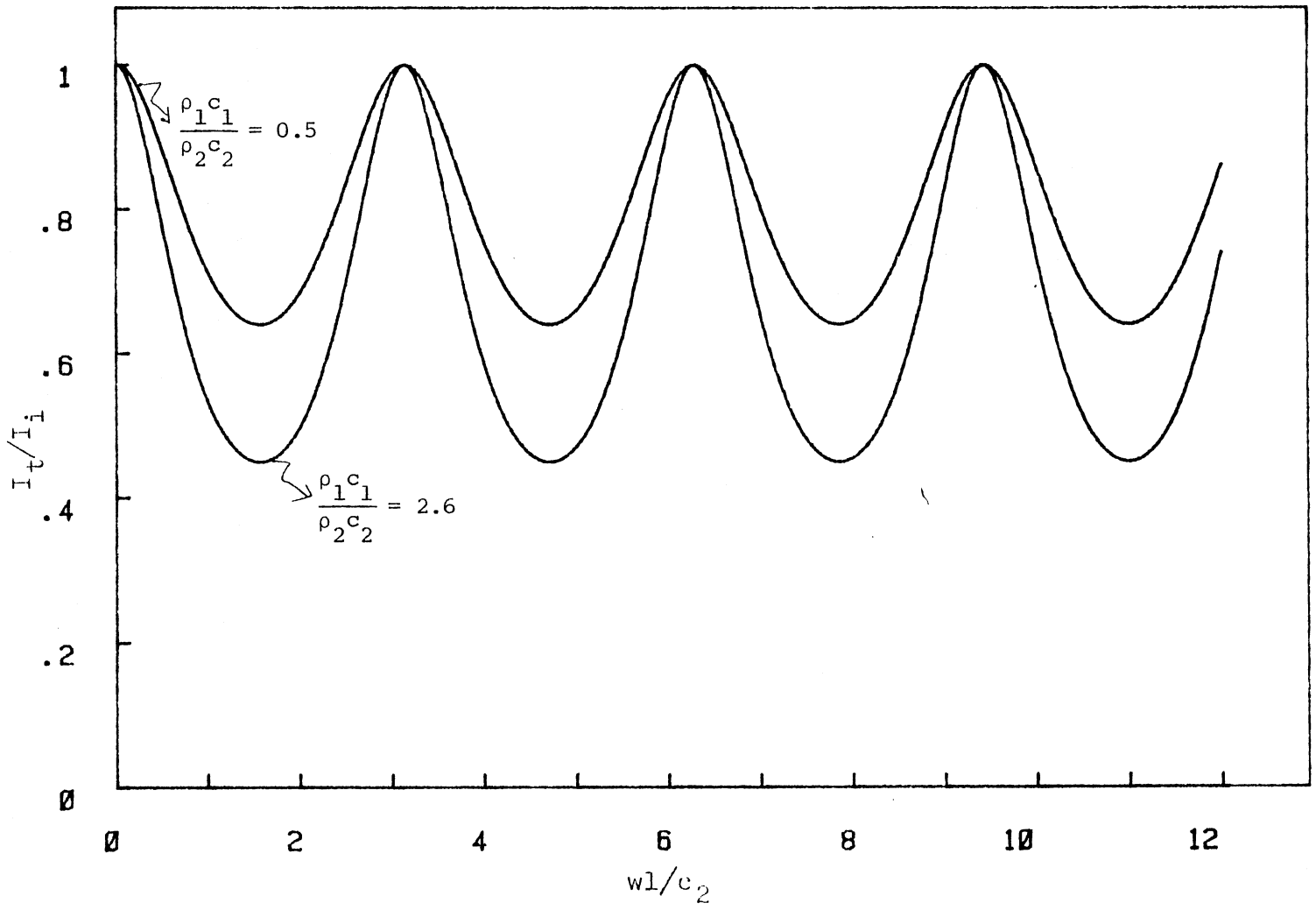

Figure 8. Change of Transmission Coefficient With Frequency

$$\nabla^2\{Qe + R\varepsilon\} = \frac{\partial^2}{\partial t^2}(\rho_{11}e + \rho_{22}\varepsilon) - \frac{\mu\Phi^2}{k}\frac{\partial}{\partial t}(e-\varepsilon) \qquad (3.20)$$

In this set of simultaneous differential equations, 'e' represents the absolute dilatation of the solid and 'ε' that of the fluid. Similarly, the basic equations that govern the propagation of pure rotational waves are (1),

$$\frac{\partial^2}{\partial t^2}(\rho_{11}\vec{\omega} + \rho_{12}\vec{\Omega}) = N\cdot\nabla\vec{\omega}$$

$$\frac{\partial^2}{\partial t^2}(\rho_{12}\vec{\omega} + \rho_{22}\vec{\Omega}) = 0 \qquad (3.21)$$

These last two equations imply a coupling between the rotation $\vec{\omega}$ of the solid and that of the fluid $\vec{\Omega}$. In Equation (3.20) and (3.21) it is assumed that the wavelength is appreciably larger than the largest dimensions of the sample's grain sizes, and that the fluid is compressible and may flow relative to the solid causing friction to arise (1).

The meaning of the various symbols used in the above equations, and symbols that will be used in the following equations, is given below:

H, P, S, Q, R = Elastic deformation constants.

N = Lame's coefficient

G_b = Shear modulus of bulk material

C_b = Bulk compressibility

C_r = Matrix compressibility

C_l = Fluid compressibility

k = Permeability

ρ = Density (with the subscripts b, 1, r corresponding to the bulk, fluid and matrix densities, respectively).

ρ_{11} = Total effective mass of the solid moving in the fluid.

ρ_{22} = Total effective mass of the fluid moving in the solid.

ρ_{12} = Mass coupling parameter between fluid and solid.

ϕ = Porosity

μ = Fluid viscosity

ω = Angular frequency

ω_c = Characteristic angular frequency

$\beta = C_r/C_b$

Now, if we consider first Equation (3.21) for the shear wave, then by eliminating $\vec{\Omega}$ in these equations, we get

$$N \nabla^2 \vec{\omega} = \rho_{11}\left(1 - \frac{\rho_{11}^2}{\rho_{11}\rho_{22}}\right) \frac{\partial^2 \vec{\omega}}{\partial t^2} . \tag{3.22}$$

This proves that there is only one type of shear waves whose propagation velocity is given by,

$$V_s = \left[\frac{N}{\rho_{11}\left(1 - \frac{\rho_{11}^2}{\rho_{11}\rho_{22}}\right)} \right]^{\frac{1}{2}} . \tag{3.23}$$

The coefficient ρ_{22} is given by Geertsma and Smit (4) as,

$$\rho_{22} = \phi^2 \rho_c \tag{3.24}$$

where ρ_c is defined by Geertsma (4) as

$$\rho_c = k \frac{\rho_e}{\phi} \tag{3.25}$$

Thus,

$$\rho_{22} = \phi\, k\, \rho_e \tag{3.26}$$

The coefficient ρ_{12} is given by,

$$\rho_{12} = \phi\, \rho_e - \rho_{22} = \phi\, \rho_e(1-k) \tag{3.27}$$

and the bulk density ρ_b is given by

$$\rho_b = \rho_{11} + 2\rho_{12} + \rho_{22}$$

Thus,

$$\rho_{11} = \rho_b - \phi\, \rho_e(2 - k)\ . \tag{3.28}$$

Substituting Equations (3.24), (3.25) into Equation (3.28) gives:

$$\rho_{11} = \rho_b - \phi\, \rho_e(2 - k) \tag{3.29}$$

Finally, substituting Equations (3.24), (3.27) and (3.29) into Equation (3.23), the shear wave velocity becomes,

$$V_s = \left[\frac{N}{\rho_b\left(1 - \frac{\rho_e}{\rho_b}\frac{\phi}{k}\right)} \right]^{\frac{1}{2}} \tag{3.30}$$

At zero frequency, that is when the coupling between the pore fluid and matrix is perfect ($k=\infty$), Equation (3.30) reduces to,

$$V_s = (N/\rho_b)^{\frac{1}{2}} \tag{3.31}$$

and when there is no coupling between the fluid and matrix, k=1, Equation (3.30) becomes,

$$V_s = \left[\frac{N}{\rho_b - \rho_e\phi}\right]^{\frac{1}{2}} \tag{3.32}$$

Equations (3.30), (3.31) and (3.32) are similar to those given by Domenico (3).

For the dilatational waves, Equation (3.20) predicts the existence of two kinds of such waves. These are denoted as waves of the first and second kind (1). The waves of the second kind are highly attenuated and have a lower velocity than the shear waves. Due to their high attenuation with increasing distance, these waves are not considered in seismic analysis. The velocity of these waves is given by Geetsma and Smit (4) as,

$$V_2 = \left(\frac{2(L\cdot H - K^2)}{\rho\cdot H}\,\frac{\omega}{\omega_c}\right)^{\frac{1}{2}} \tag{3.33}$$

where:

$$K = \frac{(1-\beta)}{(1-\phi-\beta)C_r + \phi C_e}$$

$$L = \frac{(B/C_r + 3/4\ G_b)}{(1-\phi-\beta)C_r + \phi C_e}$$

$$H = \frac{(1-\beta)^2}{(1-\phi-\beta)C_r + \phi C_e} + \left(\frac{\beta}{C_r} + \frac{4}{3}\,G_b\right) .$$

The waves of the first kind are true waves and have a higher velocity than those of the second kind. The velocity of these waves was obtained by Geertsma and Smit (4) as shown below,

$$V_1 = \left[\frac{H}{\rho} \frac{(\gamma_c + \sigma_L - 2\gamma_e \sigma_K)^2 + (\frac{\omega_c}{\omega})^2}{(\gamma_c - \gamma_e^2)(\gamma_c - \sigma_L - 2\gamma_L \sigma_K) + (\frac{\omega_c}{\omega})^2} \right] \tag{3.34}$$

where:

$$\gamma_e = \frac{\rho_c}{\rho}, \ \gamma_c = \frac{\rho_c}{\rho}, \ \sigma_K = \frac{K}{H}; \ \sigma_L = \frac{L}{H} .$$

From Equation (3.34), letting ω approach zero, we find

$$V_{1(\omega=o)} = (\frac{H}{\rho})^{\frac{1}{2}} = \{\frac{1}{\rho}[\frac{(1-\beta)^2}{(1-\phi-\beta)C_r + \phi C_e} + \frac{\beta}{C_r} + \frac{4}{3} G_b)]\}^{\frac{1}{2}}$$

Note that in this equation the velocity is independent of the frequency. Now, if we let ω go to infinity in Equation (3.34), then,

$$V_{1(\omega \to \infty)} = \{\frac{H}{\rho} \frac{(\gamma_c + \sigma_L - 2\gamma_2 \sigma_K)^{2\ \frac{1}{2}}}{(\gamma_c - \gamma_e)^2}\}$$

These last two equations are similar to those given by Domenico (3).

CHAPTER IV

RESULTS AND DISCUSSION

Physical Characteristics of the Sandstone Samples

In general, sandstone matrix is composed of: sand grains cemented together with clay elements, and pores of different shapes and sizes randomly distributed over the matrix. Due to this, the sandstone samples in this experiment are characterized by the distribution of their grain sizes, their porosities, the elements composing each sample's matrix, and the clay minerals.

The grain sizes are found by scraping sand particles from each sandstone sample, and measuring their diameters with the help of a microscope. In Figure 9, histograms of the grain sizes for the experimental samples are shown. From this figure it is clear that the diameters of the sand grains fall between 0.1 mm to 0.3 mm. With grains of diameters 0.1 mm to 0.2 mm being the most dominant for most samples.

The porosity of each sample was found by following the procedure outlined in Chapter II, and are recorded in Table III. It is clear that this experiment's sandstone samples vary over a wide range in their porosities. In Figure 10, a plot of the compressional velocity versus the porosity (at zero pressure) for the experimental sandstone samples is shown. It is apparent that the best curve that fits the experimental

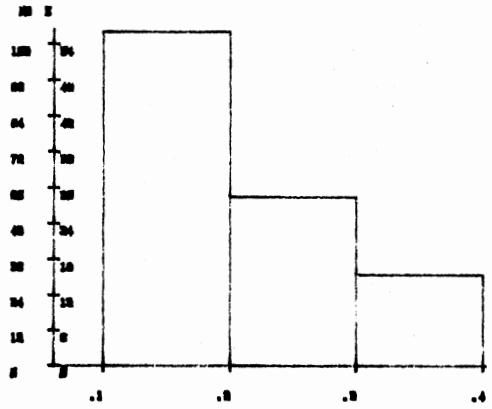

a.) Sample 4

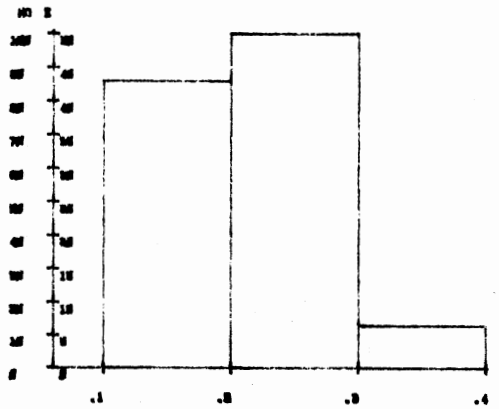

b.) Cockran Sample

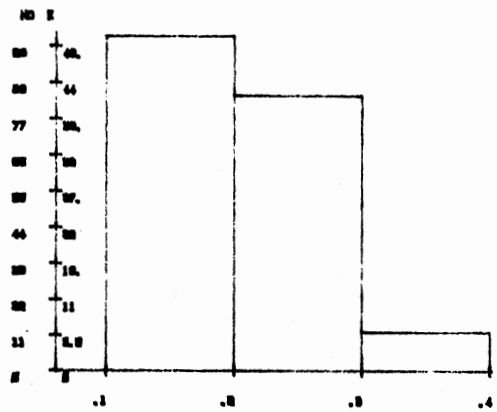

c.) Mesa Sample

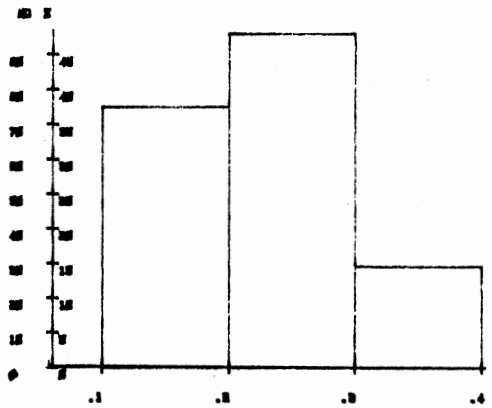

d.) Sample 1

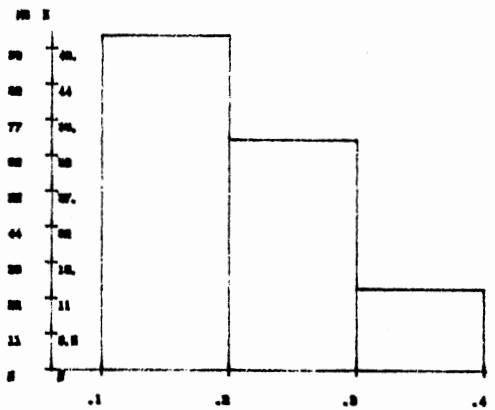

e.) Sample 2

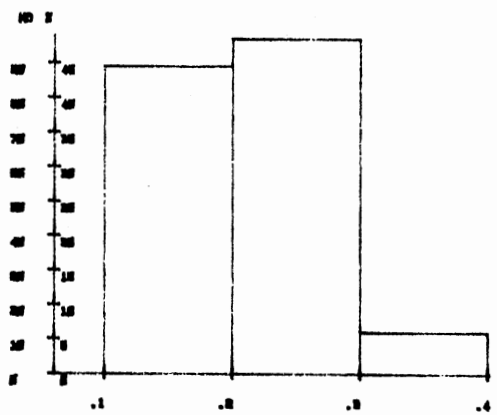

f.) Sample 3

Figure 9. Histograms For The Sand Grains' Distribution Of The Experimental Samples

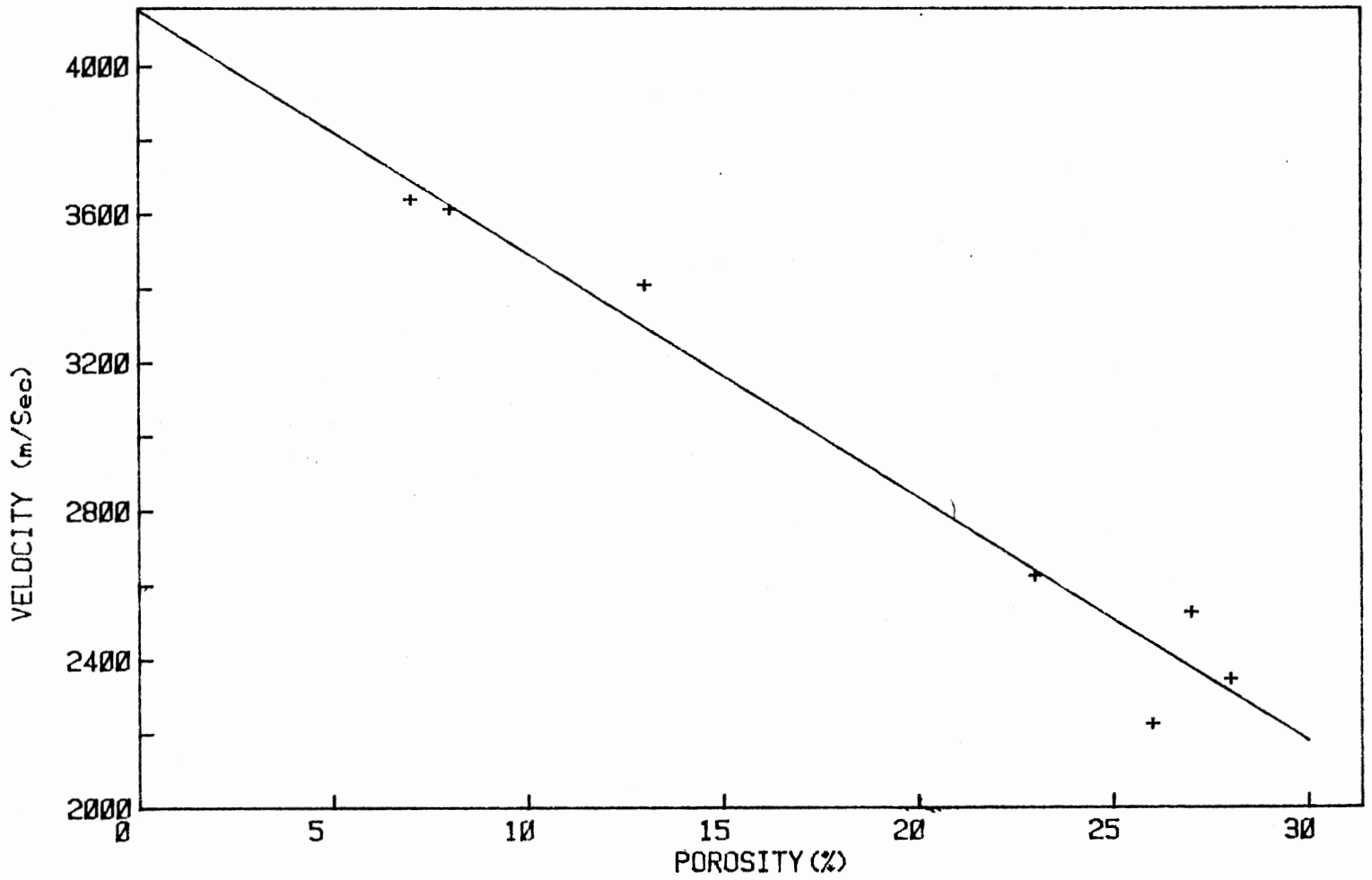

Figure 10. Compressional Velocity Verses Porosity For The Sandstone Samples

points is a straight line, and that as the porosity increases the velocity decreases, as expected from Equation (2.1).

The elements composing each sample were detected by using the X-ray diffraction analyses. This analysis gave: the energy spectrum of each sandstone sample, the element corresponding to each energy, and the area under each element's energy peak. The percent abundance of each element was found by dividing the area under that element's energy peak by the total area under all energy peaks. Table I shows the elements present in each sample and their percent abundances. As seen in this table, all the experimental samples have silicon as the most dominent element, that is they are quartz rich subarkorkoses, containing approximately 70 percent quartz, with the other elements representing the cementing materials and clays. To investigate more about the kind of clays present in each sample, a scanning electron microscope was used to determine the morphology and textural relationships of these clays. Pictures taken from this analysis were compared to those given by Wilson and Collaborates (18). The clay minerals present in each sample were determined from these pictures, and the relative abundance of the following elements (18): aluminum (kaolinite), potassium (illite), iron or magnesium (chlorite), and calcium or sodium (smectite). Table II shows the clay minerals believed to be present in each sandstone sample. Note that all of the samples have more than two types of clay minerals in them.

In general, we can conclude that this experiment sandstone samples are very fine grained, well sorted, quartz rich, contain small amounts of clay and can be regarded as clean.

TABLE I

THE PERCENTAGE ABUNDANCE OF SANDSTONE ELEMENTS

Sample	Elements							
	Si	Al	Cl	Fe	K	Ca	S	Mg
1	90	5	2	1.6	1.4			
4	67	1	0.4	2	1	28		0.5
3	96	1	1	1	1			
2	85	6	1	4	3	1		
Cockran	75	5		3	5	11	1	
Mesa	89	3		3	3	2		

TABLE II

CLAYS IN THE SANDSTONE SAMPLES

Sample	Clays				
	Kaolinite	Illite	Chlorite	Smectite	Hemitite
1	Yes	Yes	Yes	No	No
2	Yes	Yes	Yes	Yes	No
3	Yes	Yes	No	Yes	No
4	Yes	Yes	No	No	Yes
Cockran	Yes	Yes	Yes	Yes	Yes
Mesa	Yes	Yes	Yes	Yes	Yes

Preliminary Results

Preliminary experiments were performed to determine the velocity of seismic pulse in water. The value of this velocity was determined by finding the time it takes a seismic pulse in water to traverse a known distance. Plotting a distance versus time graph (Figure 11), and taking its slope we find the desired velocity. In this experiment, the average value for a seismic wave's velocity in water, at room temperature and atmospheric pressure, was 1504 m/sec. This value is in very good argument with the value given by Temkin (13) at $25^{o}C$ (1497 m/sec), where the percent error between the two values is 0.5%.

The absolute accuracy of the velocity measurements, as carried in this experiment, was tested by using an aluminum block of known thickness and measuring its dilatational wave velocity. First, this velocity was measured by placing the piezoelectric crystals directly on two opposite faces of the block and recording the time of flight of the seismic pulse. The average velocity, in the aluminum block using this method, was found to be 6424 m/sec. Next, the aluminum block was put inside the water tank and the velocity was measured in two directions using the methods outlined in Chapter II. The values found were 6132 m/sec and 6258 m/sec. The conclusions from these measurements are:

1. There is a 5% error introduced in the measurement inside the water tank.

2. Using the two sets of hydrophones to record the time of flight of the seismic pulse, as explained in Chapter II, the recorded velocities found by using Equations (2.3) and (2.4), respectively, differ by 2 percent. This error is within the expected experimental error, which

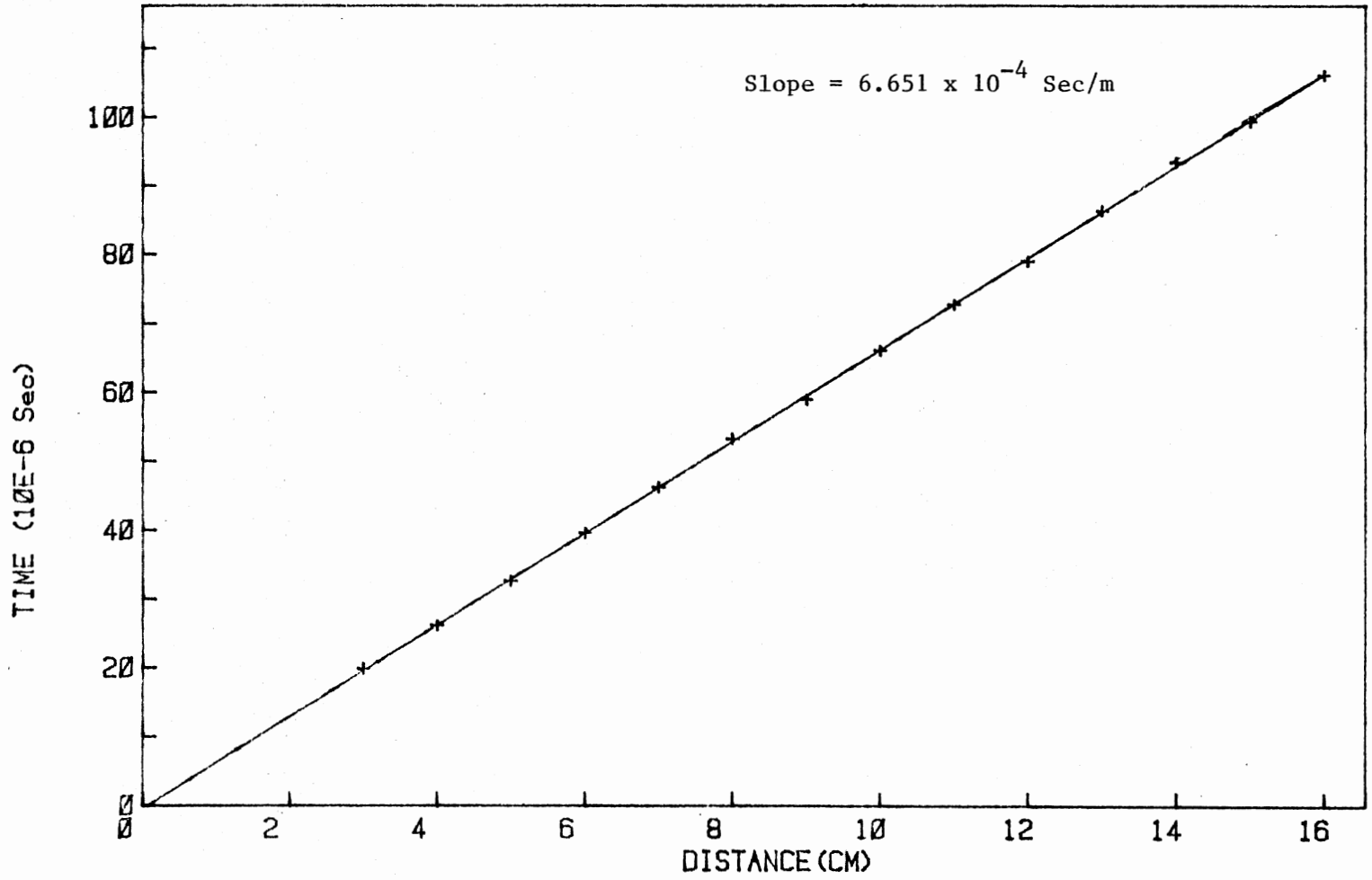

Figure 11. Time Of Flight Of A Seismic Pulse In Water Verses Distance

will be discussed later.

Sandstone samples were also used to check if the velocity measurements found by using the two sets of hydrophones (as explained in Chapter II) give the same value; provided the velocity with both methods is measured either parallel or perpendicular to the sample's bedding planes. It was found that the velocities found by both methods agree to less than one percent difference, which is well within this experiment's expected error. This part of the experiment established the degree of accuracy and reliability of this experimental set up.

Next, the reproducibility of the measurements was tested by taking each sandstone sample through the aspiration process, recording its velocity and mass, then carrying the same cycle again. It was found that for the same saturation level, the velocities were reproducible to within one percent error.

An error analysis, as shown below, illustrates the expected experimental relative error. Using Equation (2.3) we get:

$$V_1(1\pm\delta) = \frac{D_1\cdot(1\pm\delta_1)}{t_2(1\pm\delta_2) - t_1(1\pm\delta_3)} .$$

Where the δ's are the expected errors in the quantities they are multiplied with. V_1, D_1, t_1 and t_2 represent the same parameters as explained in Chapter II. Using sample 4 as an example where: $D_1 = 4.80$ cm, $t_2 = 5.5553 \times 10^{-6}$ sec and $t_1 = 26 \times 10^{-6}$ sec. It is found that, $\delta_1 = (0.05 \text{ cm}/D_1)\times 100 = 1\%$, $\delta_2 = (0.05 \times 10^{-5} \text{ sec}/t_2) \times 100 = 0.9\%$ and $\delta_3 = (5 \times 10^{-8} \text{ sec}/t_1) \times 100 = 2\%$. Using the fact that relative errors in a produce or a quotient equals the sum of the relative errors in the input equation, it is found that $\delta = 2\%$. That is, the calculated maximum

relative error in the sample's velocity is 2%. However, taking different measurements for this sample's compressional wave velocity, it was found that the relative error between them is 0.1%. For the other samples this error goes up to about 1.5% (as long as the saturation level is the same from one run to the other). For sample 1, it was found that when the saturation level changed by 2%, this caused the velocity to change by 4%, from 2070 m/sec to 2151 m/sec. This example illustrates that the saturation level of sandstone does indeed effect its compressional wave velocity.

Thus, this part of the experiment establishes that the reproducibility of the measurements is well below the expected experimental error, as long as the saturation of the sample does not change.

Velocity-Time Dependence

When each sandstone sample was taken out of the desiccator and put into the water tank for the velocity measurement, it was observed that the time of flight of the seismic pulse through the sample decreased for the first 35 to 60 minutes and then remained constant. This means that the velocity increased and reached a value where it stabilized. This behavior is shown in Figures 12, 13 and 14 for the sandstone samples 1, 4 and 5. For sample 1, it took 50 minutes before the value of the velocity stabilized, during which time there was a 10% increases in the compressional wave velocity. For sample 4 there was a 3% increase in the velocity for the first 45 minutes, then the value of the velocity stabilized. For sample 5 there was a 7% increase in the compressional wave velocity during the first forty minutes. This increase in the velocity is due to the change in the sample's environment. While in the desicca-

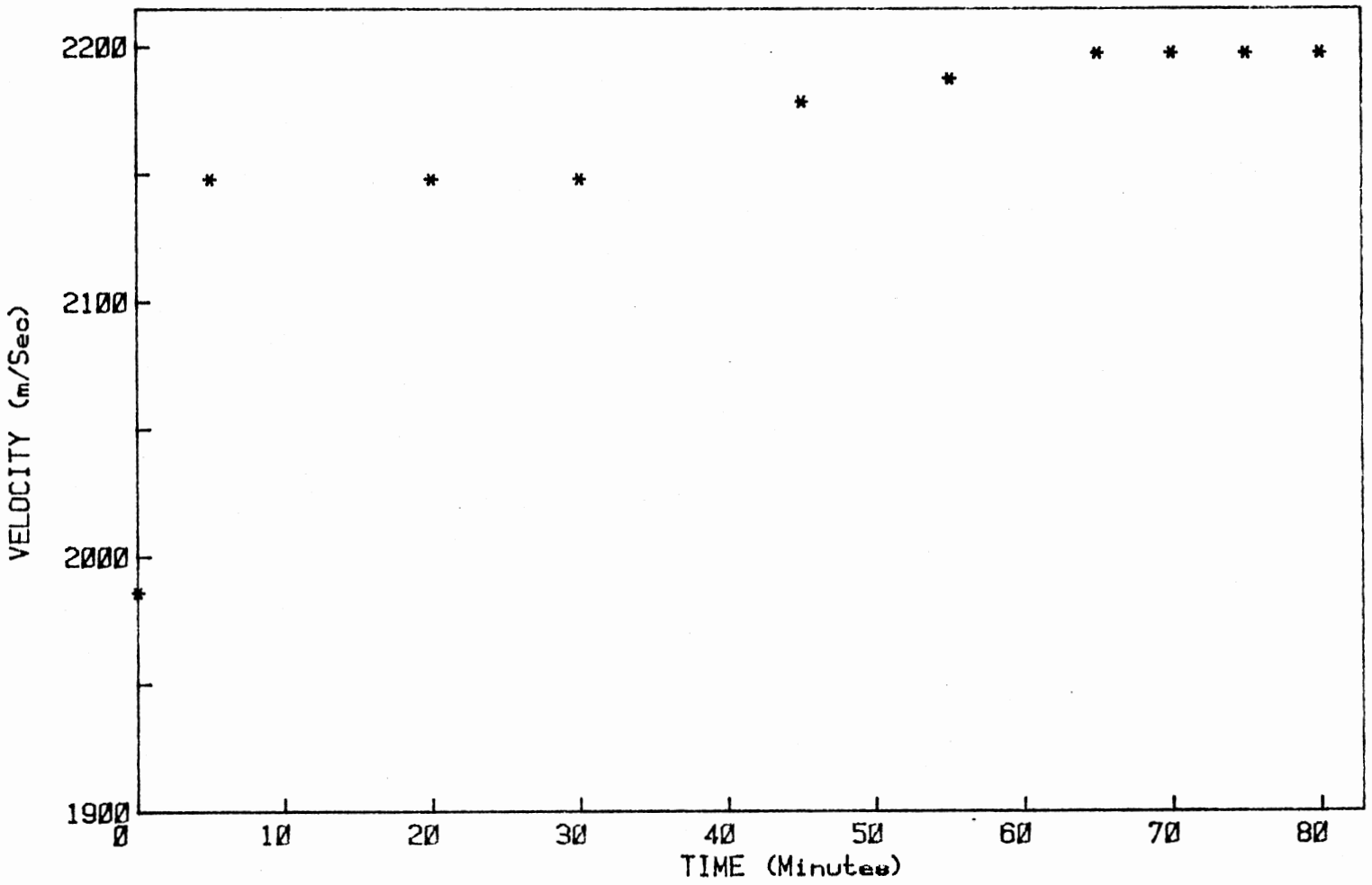

Figure 12. Change Of P-Wave Group Velocity With Time For Sandstone Sample 1

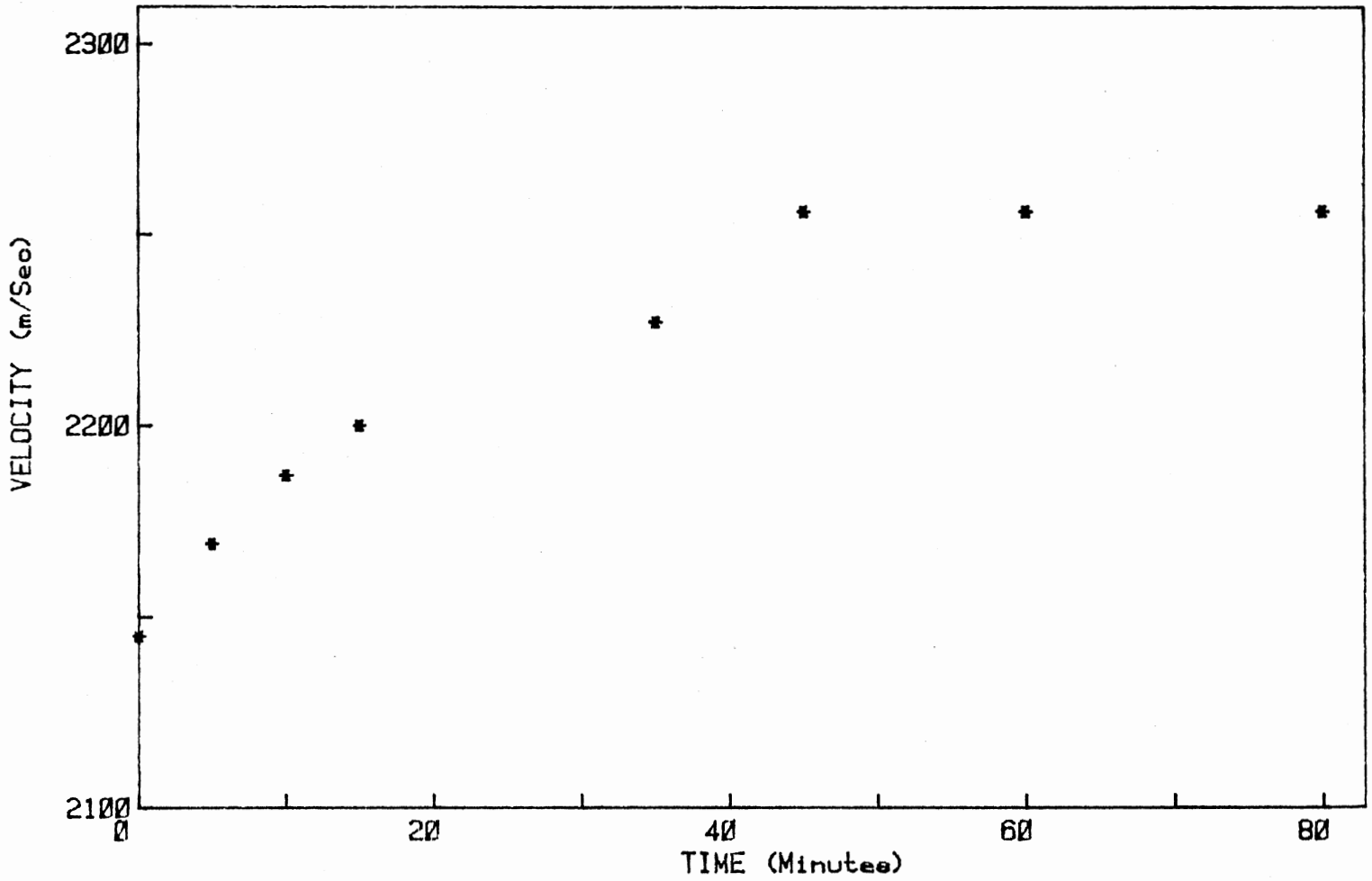

Figure 13. Change Of P-Wave Group Velocity With Time For Sandstone Sample 4

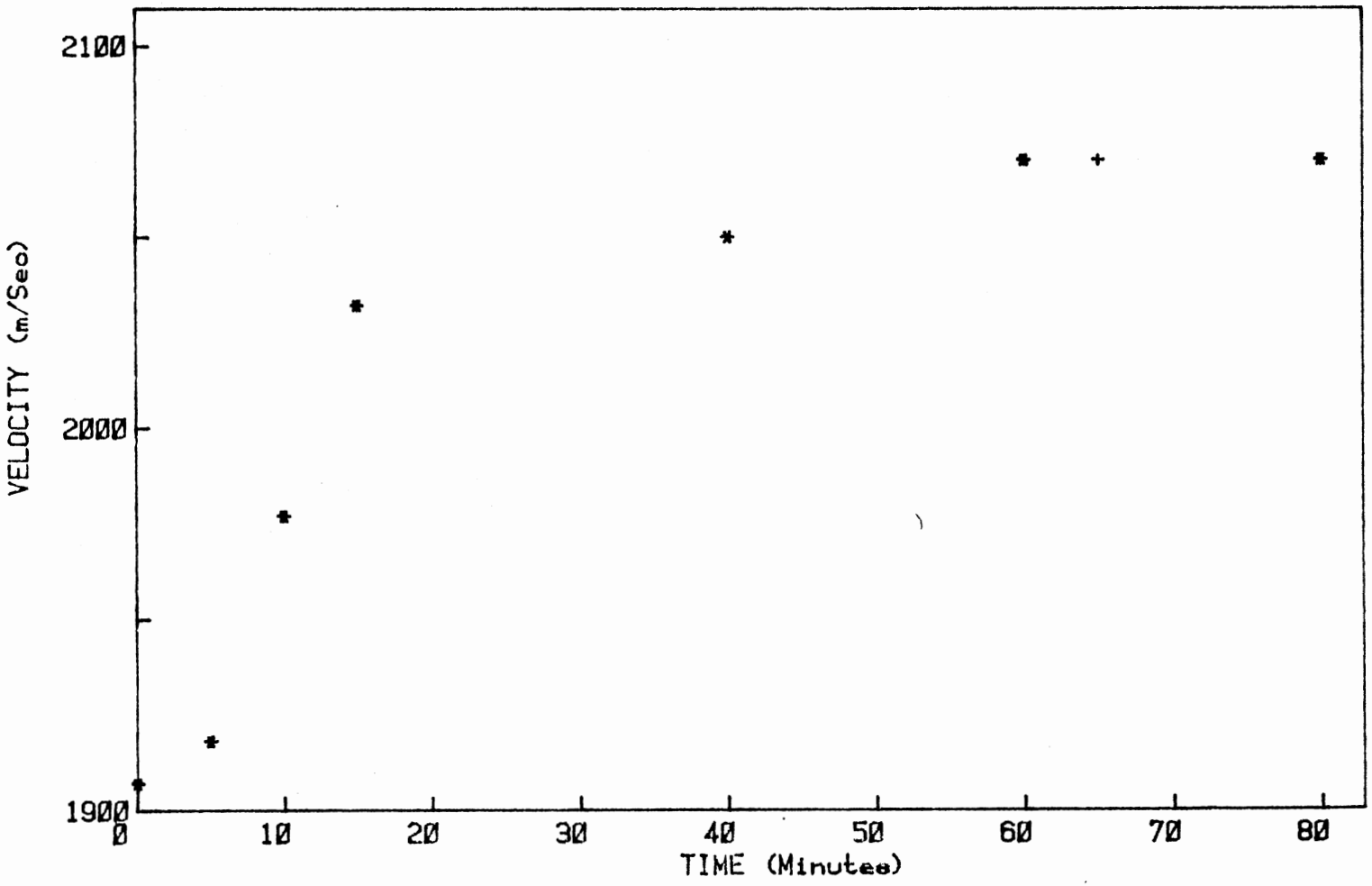

Figure 14. Change Of P-Wave Group Velocity With Time For Sandstone Sample 5

tor, the sample was surrounded by aspirated water at 21°C. However, when placed in the water tank the surrounding water was nonaspirated and at room temperature (23°C). The moving of the sample from desiccator to water tank caused the formation of air bubbles on the sample's surface (as observed by a microscope). These air bubbles increased in size over time and, after having reached a certain volume, escaped from the sample's surface.

This part of the experiment shows that before any experimental measurements, the sandstone samples should be left inside the water tank for about one hour, during which time the sample reaches an equilibrium with its surroundings.

Velocity-Frequency Dependence

The effect of the seismic wave frequency on the velocities in saturated sandstone samples was investigated by taking each velocity measurement at two frequencies, 20k Hz and 200k Hz. The velocities were recorded as the uniaxial stress on the sample was being increased. It was observed that for most of the experimental samples there was a hystoresis effect, with higher velocities being recorded after the first pressure cycle. The difference in velocities due the hysteresis effect was mostly observed at low values of the applied stress (zero to 500 psi) and this difference ranged from 1 to 7 percent depending on the sample. However, for all the samples used in this experiment the hysteresis effects diminished after running the sample through two cycles of pressure.

Figures 15, 16, 17 and 18 show the change of velocity in the direction of the applied stress for both frequencies (20k Hz and 200k Hz).

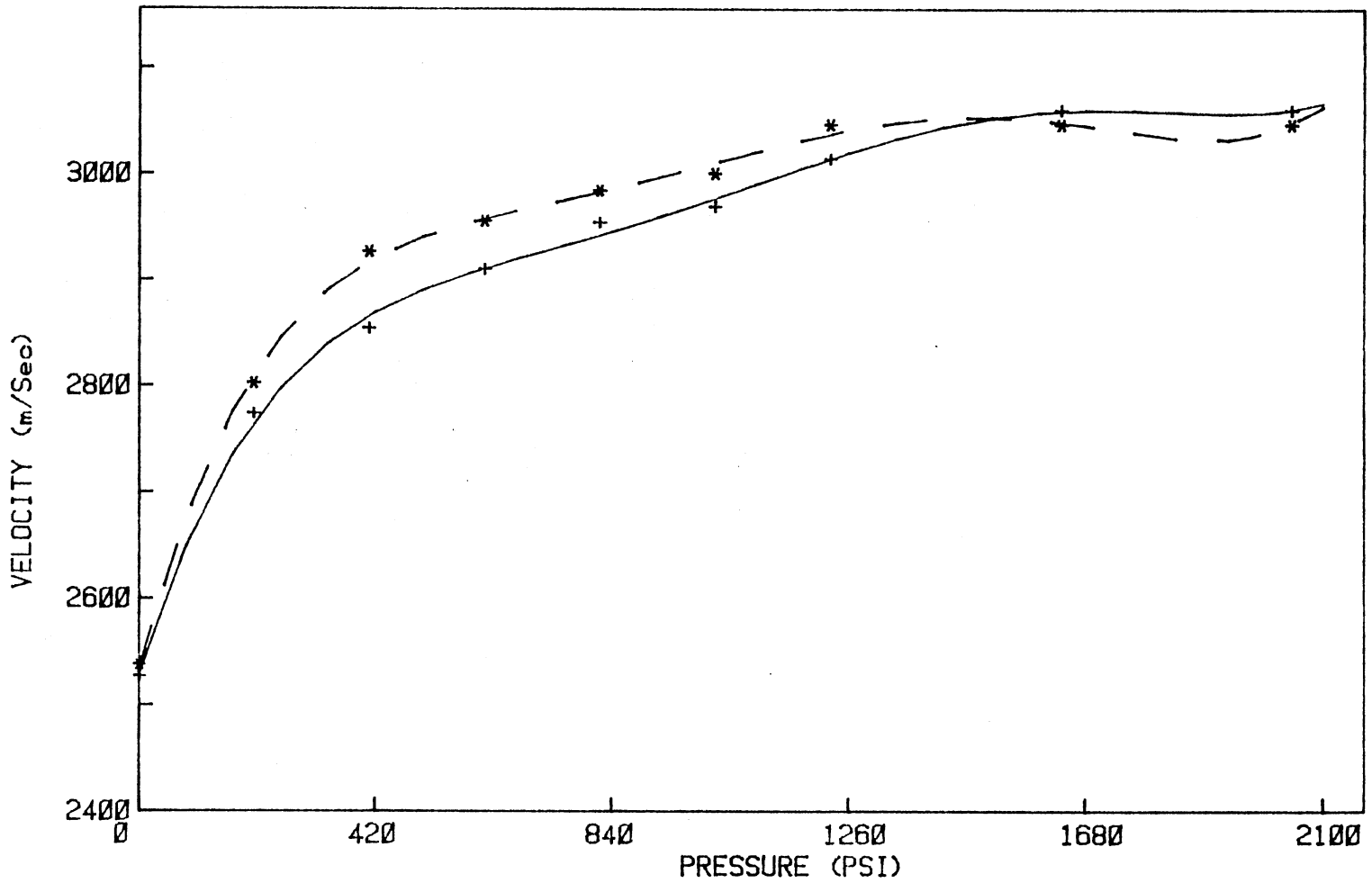

Figure 15. Change Of Velocity With Frequency For Sandstone Sample 1

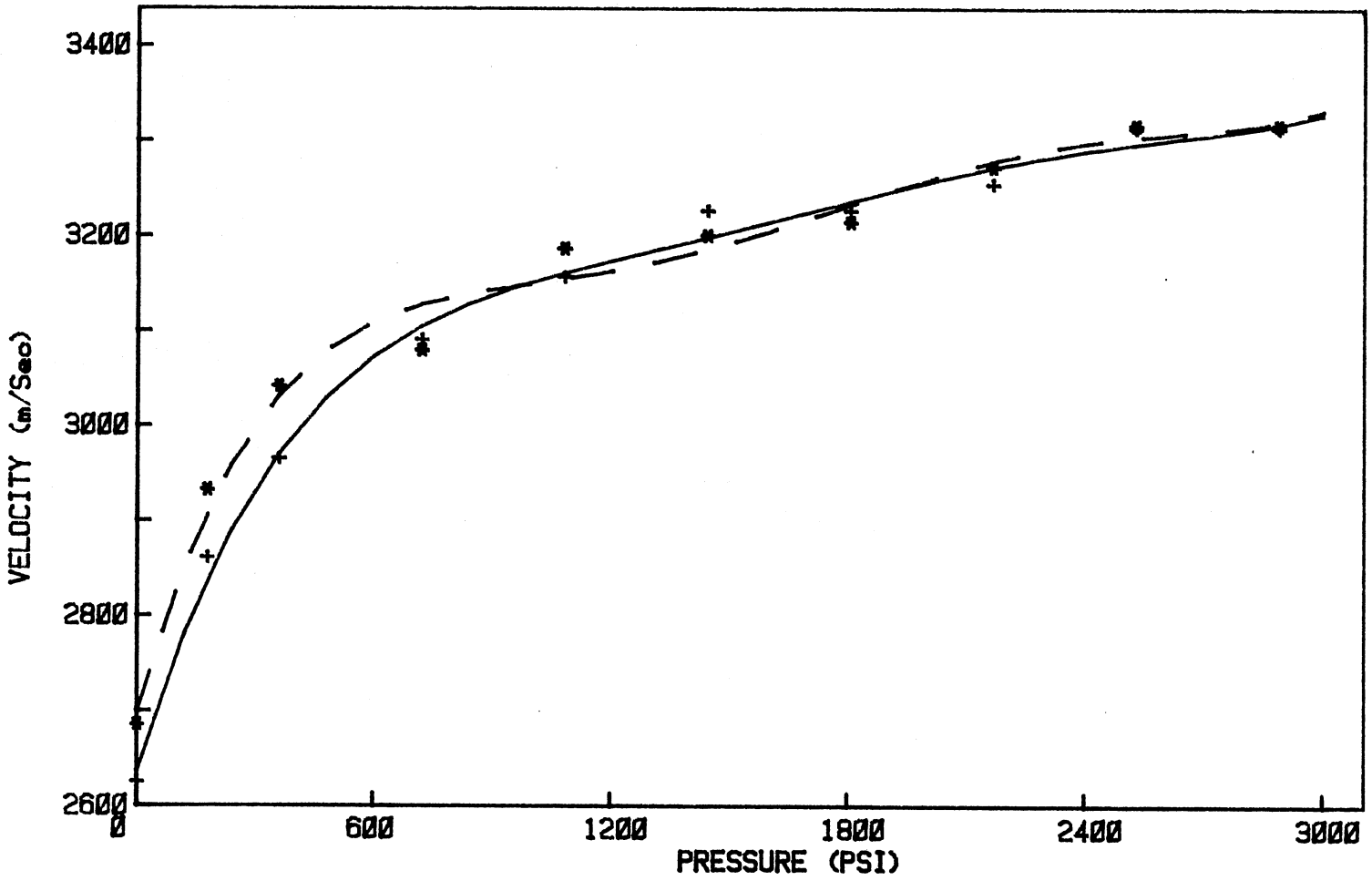

Figure 16. Change Of Velocity With Frequency For Sandstone Sample 2

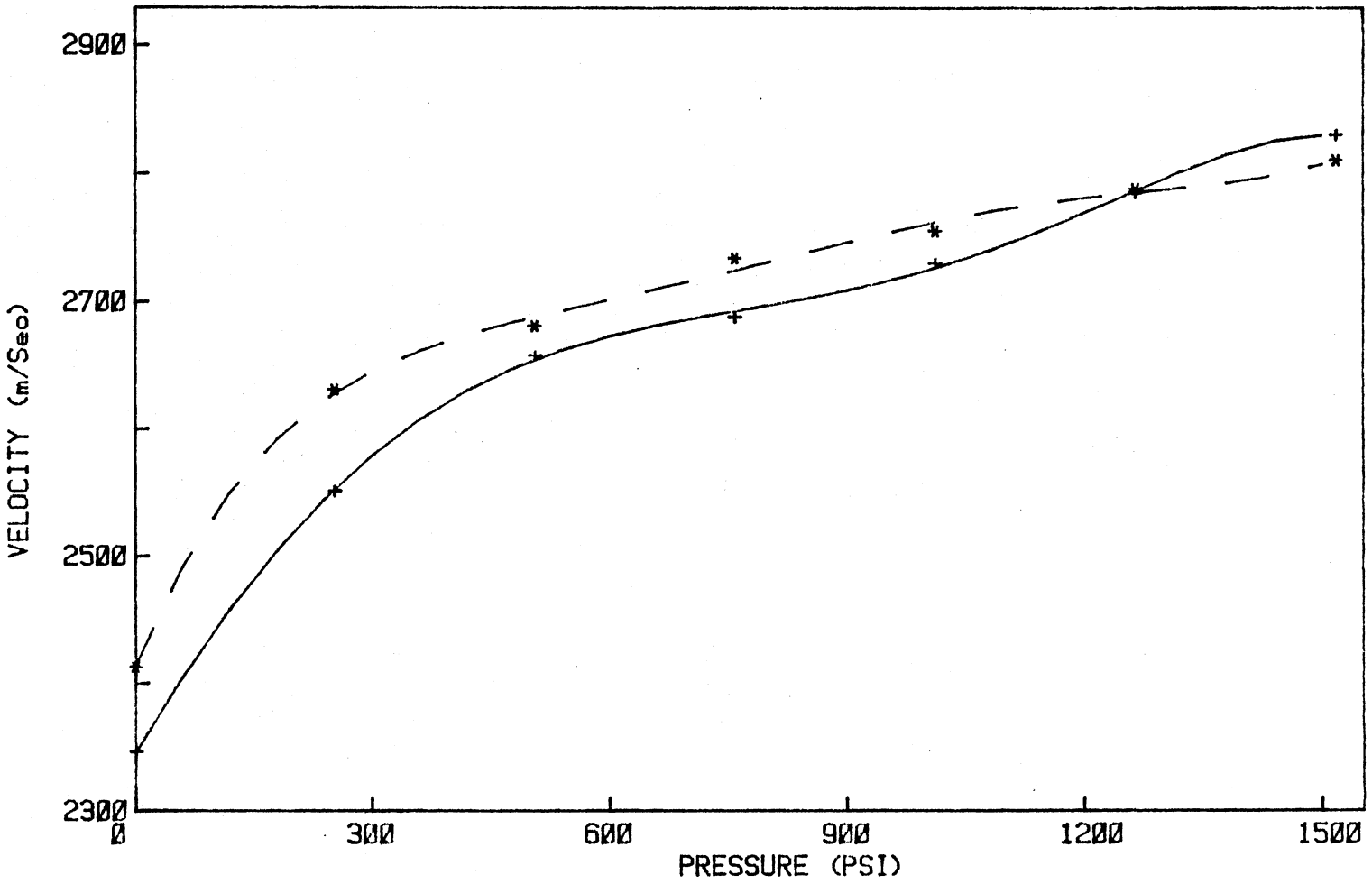

Figure 17. Change Of Velocity With Frequency For Sandstone Sample 4

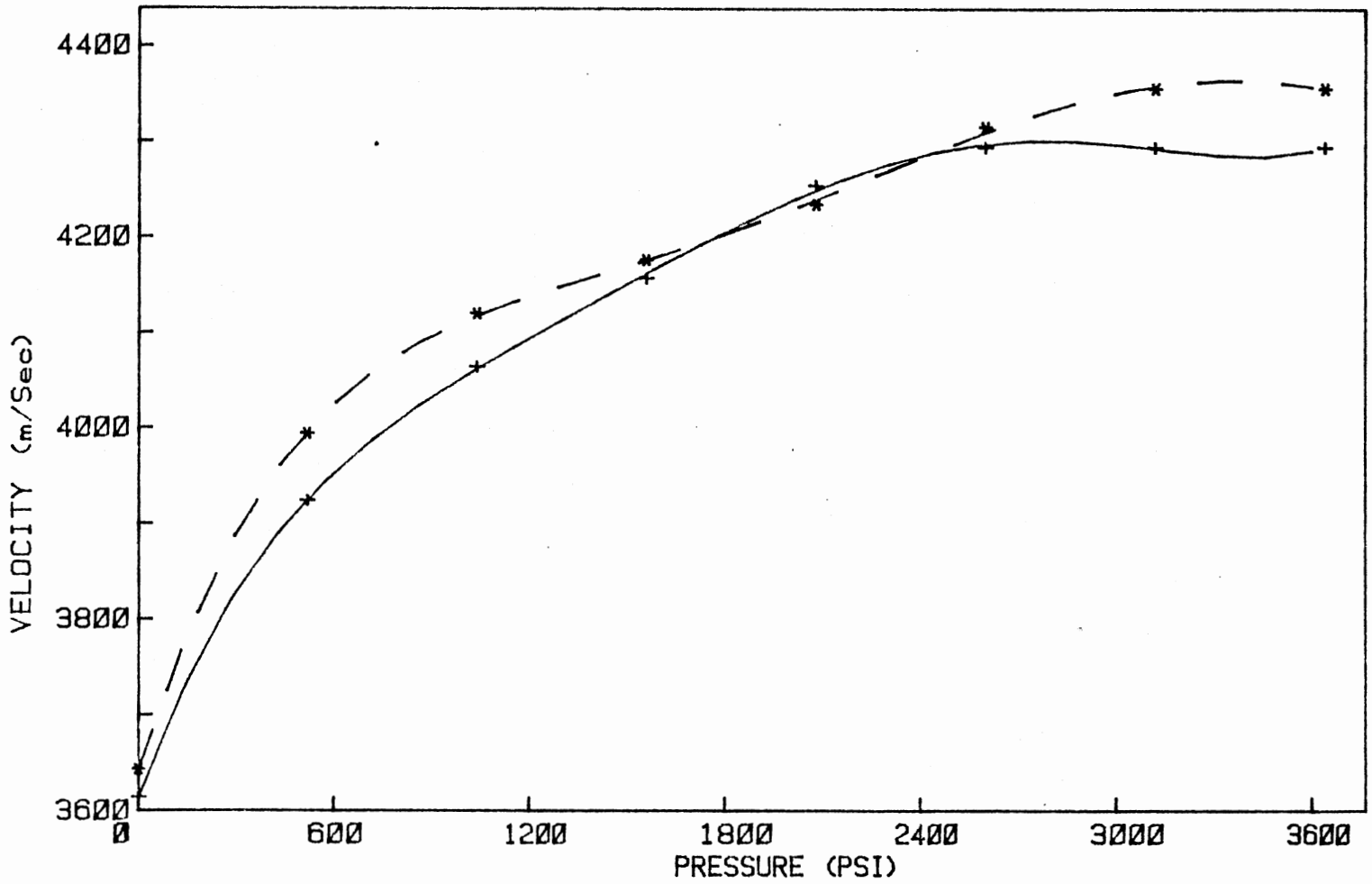

Figure 18. Change Of Velocity With Frequency For The Mesa Sandstone

The stress was applied perpendicular to each sample's bedding planes. In these figures, the solid curves represent those measurements made at 20k Hz, while the dashed curves stand for those measurements at 200k Hz. All the curves were plotted by interfacing an x-y plotter to the H-P 85 minicomputer; then executing a polynomial curve fitting program through the data points.

Analyzing the frequency dependence of each sample, it was found that for stresses above 1200 psi, the percent difference between the velocities at 20k Hz and 200k Hz (for all of the experimental sandstone samples) fell within the expected experimental error. However, for low stress values (those below 1200 psi), it was hard to distinguish if the percent difference was due to experimental error or to the change of velocity with frequency. At zero applied stress, sample 4 (Figure 17) shows a 4% difference between the velocities at the two frequencies. As the applied stress increased this percent difference decreases to fall within the expected experimental error, at about 1000 psi. The rest of the samples (Figures 15, 16 and 18) show that the percent difference between the velocities, at all the applied stress values is well within (or close) to the expected experimental error.

From the above analysis we can conclude that the velocity of a seismic pulse in sandstone does not show any detectable frequency dependence.

Pressure-Velocity Dependence

The velocities in the direction of and perpendicular to the direction of the applied stress were recorded at least five minutes after each stress value was applied. The change of these velocities (at 20k

Hz) with increasing stress is shown in Figures 19, 20, 21, 22 and 23 for sandstone samples 1, 2, 4, Cockran and Mesa, respectively. In these figures, the solid curves represent the measurements in the direction of the applied stress; while the dashed curves represent measurements perpendicular to the direction of the applied stress.

The information gathered from analyzing these figures is shown in Table III. The first row in this table shows the measured porosities. The second row shows the anisotropy in each sample, this is calculated by taking the ratio between the two velocities, with the higher velocity in the numerator. This ratio is defined here as the anisotropy factor. The number in parenthesis (in this row) corresponds to the percent difference between the two velocities. The anisotropy factor is calculated both at zero stress and at each sample's maximum applied stress. The reason behind this is to discover the effect of the applied uniaxial stress on the anisotropy. The third row gives the percent increase in the velocity perpendicular to each sample's bedding planes, resulting from the maximum applied pressure. The number in parenthesis gives the ratio by which this velocity increases. Similarly, the last row shows the percent increase in the velocity parallel to the bedding planes resulting from the maximum applied uniaxial pressure. The number in parenthesis gives the ratio by which this velocity increases.

The following conclusions are drawn from Table III and the last five figures:

1. The samples used in this experiment are inherently anisotropic. The degree of anisotropy varies from 1.01 to 1.05 (shown in Table III), with three of the samples having an anisotropy factor of 1.05 when the applied pressure is zero.

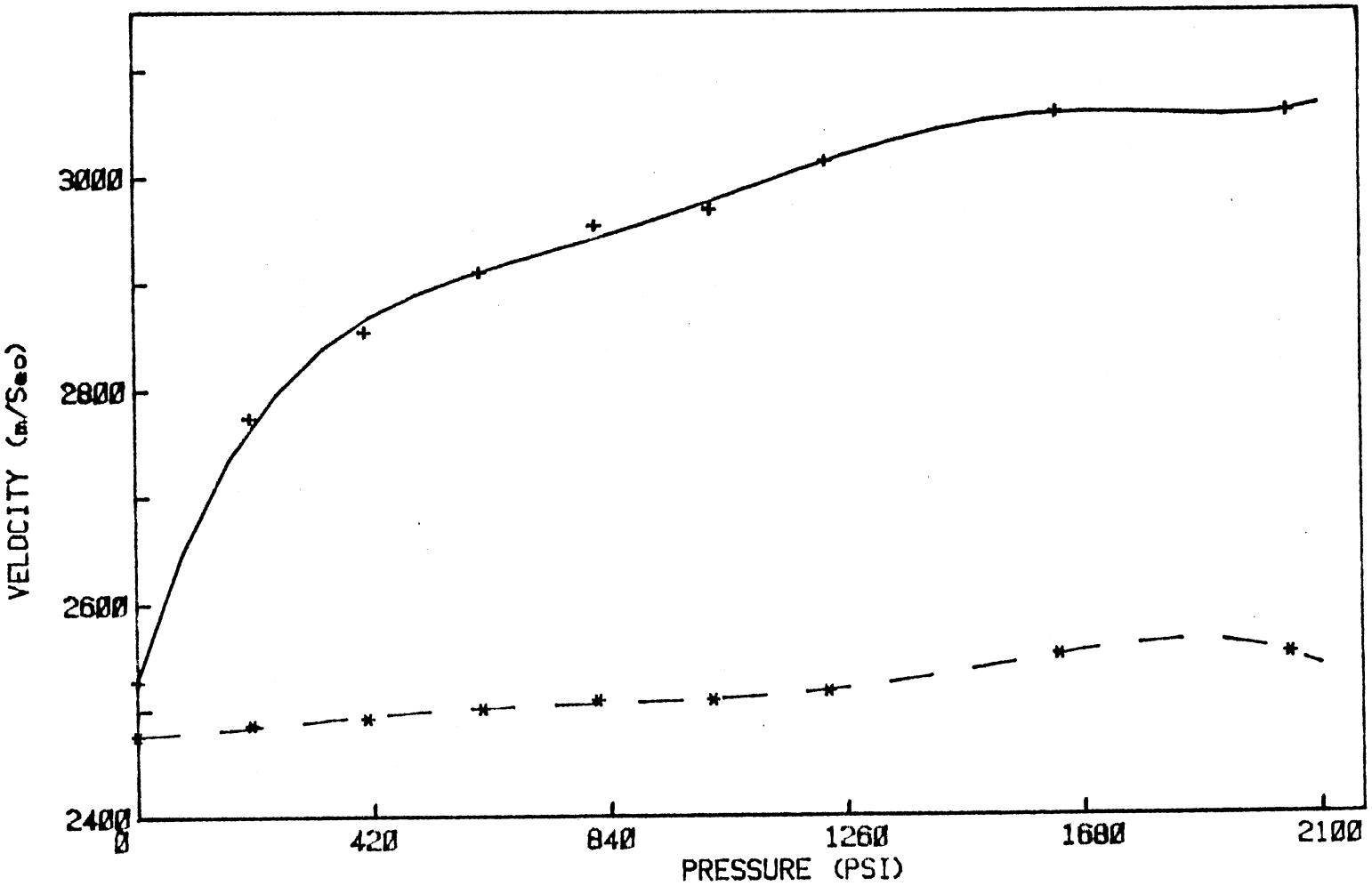

Figure 19. Velocity Verses Applied Stress For Sandstone Sample 1

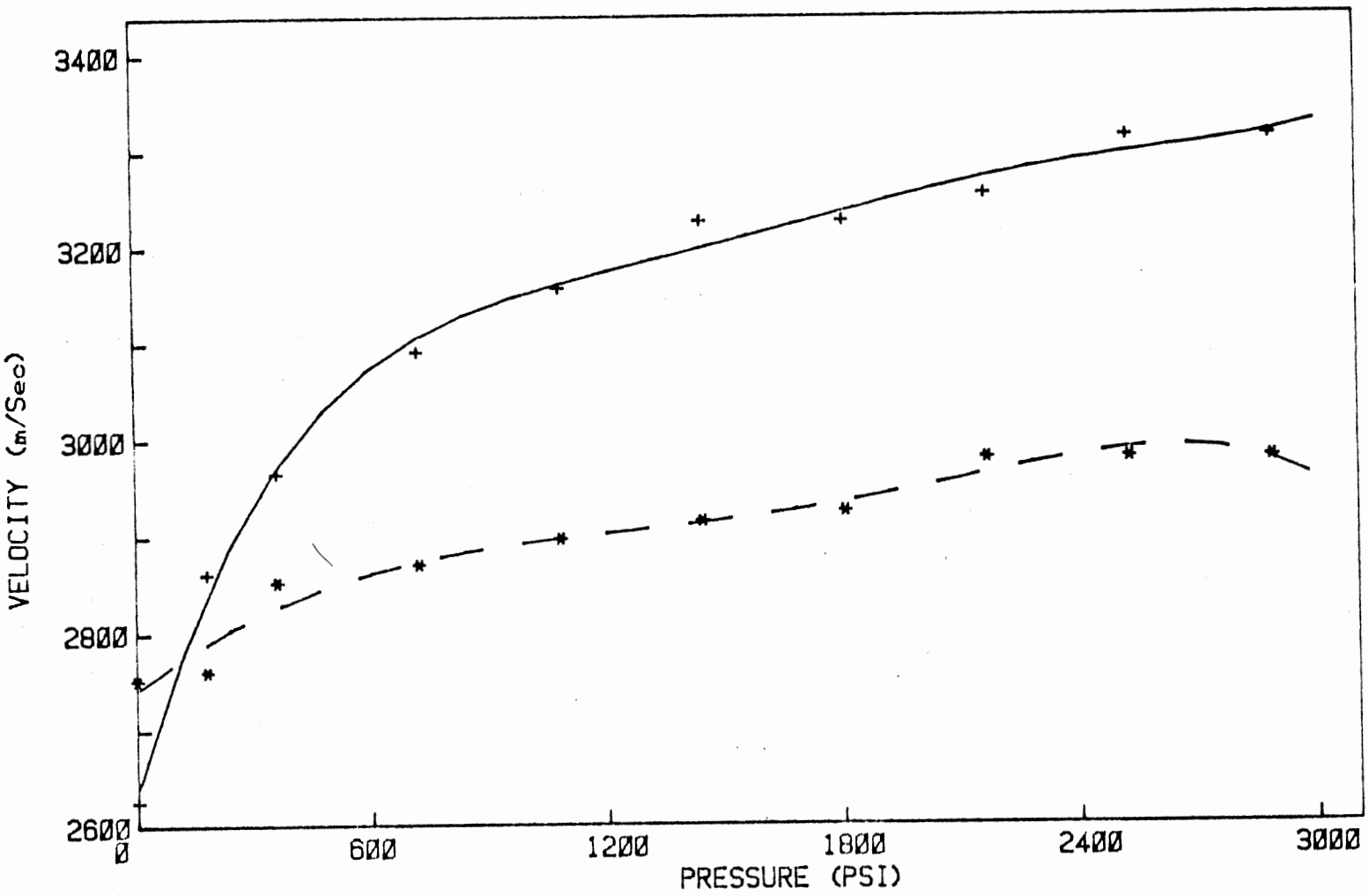

Figure 20. Velocity Verses Applied Stress For Sandstone Sample 2

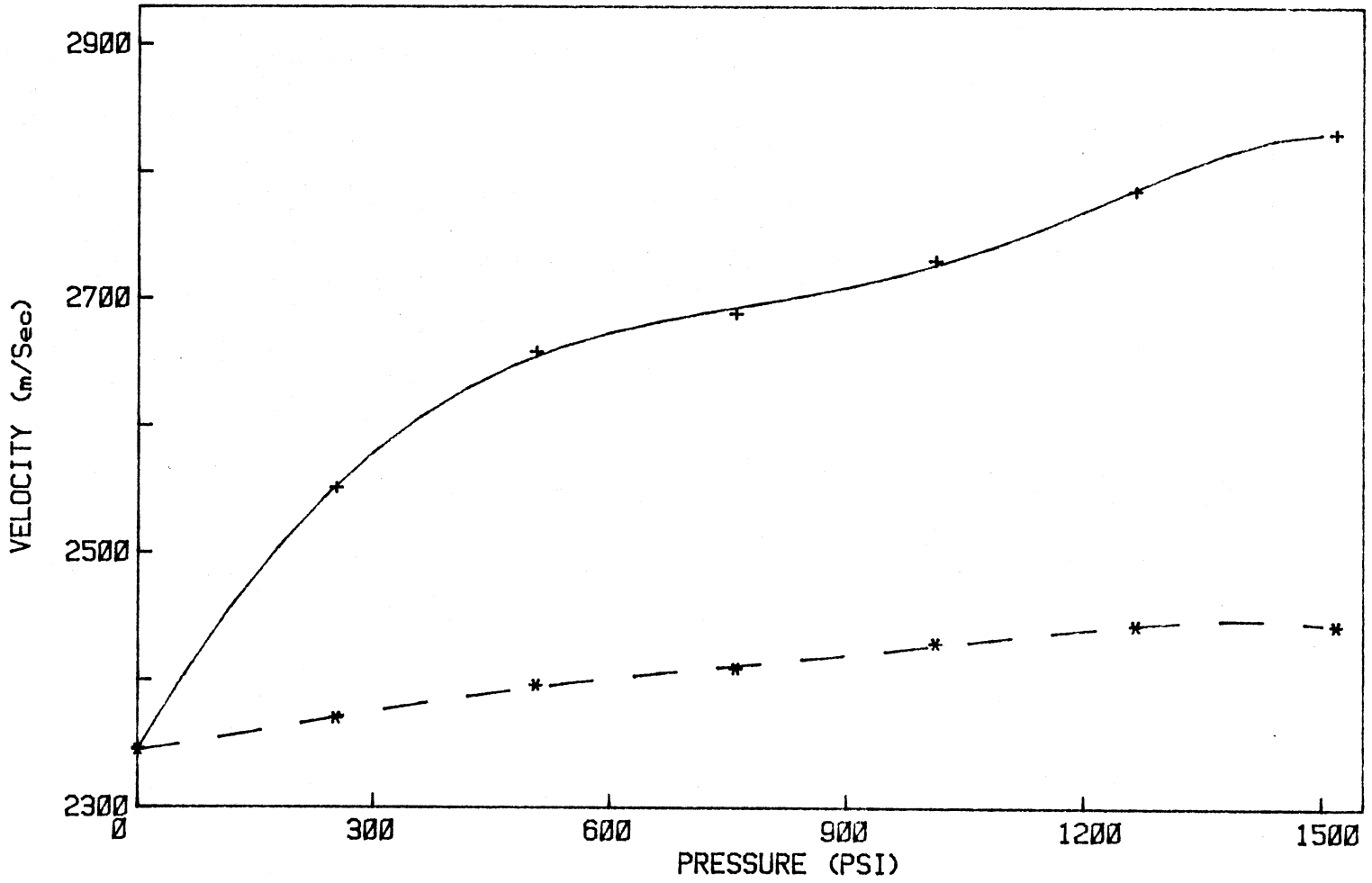

Figure 21. Velocity Verses Pressure For Sandstone Sample 4

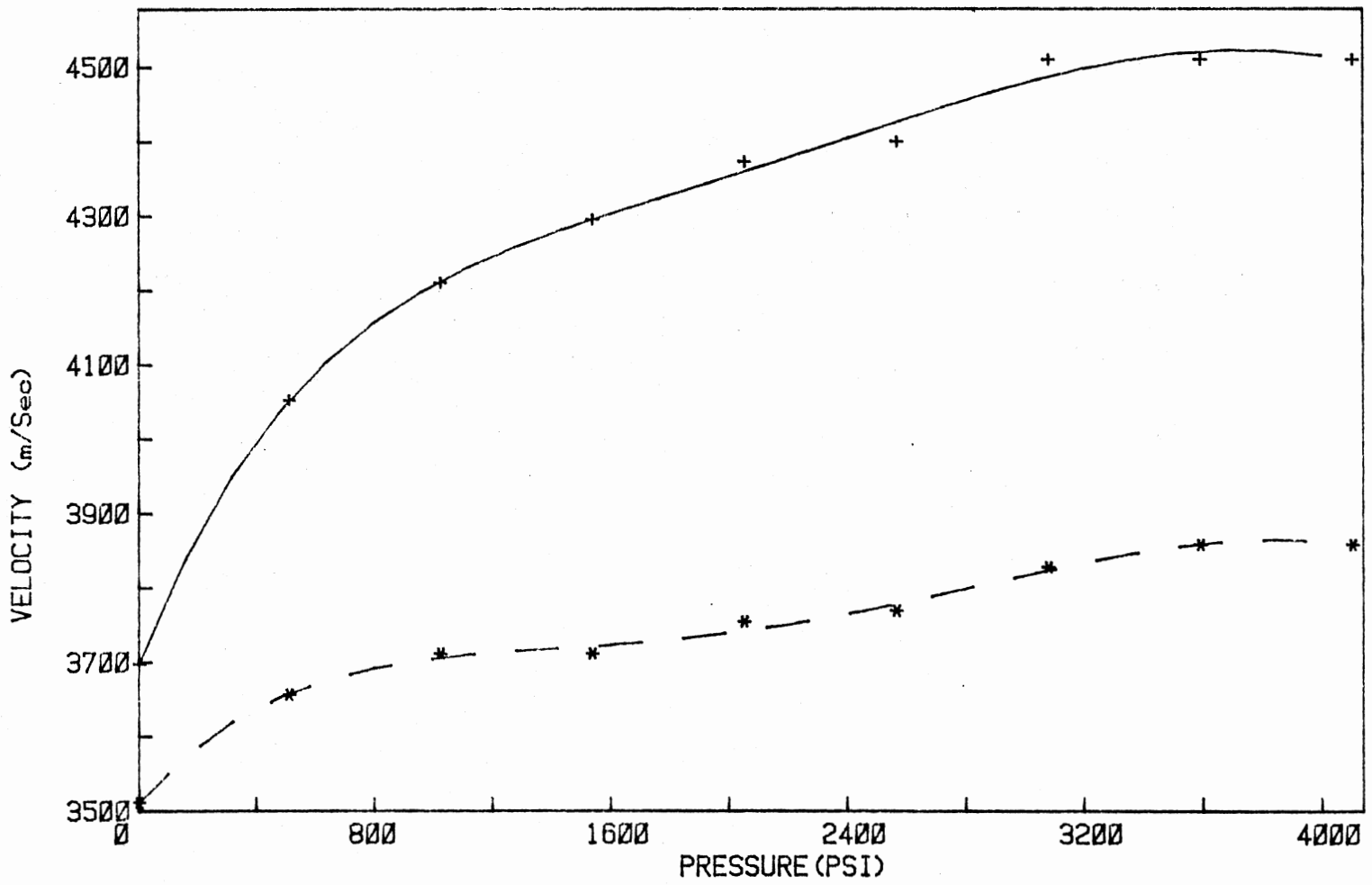

Figure 22. Velocity Verses Applied Stress For The Cockran Sandstone

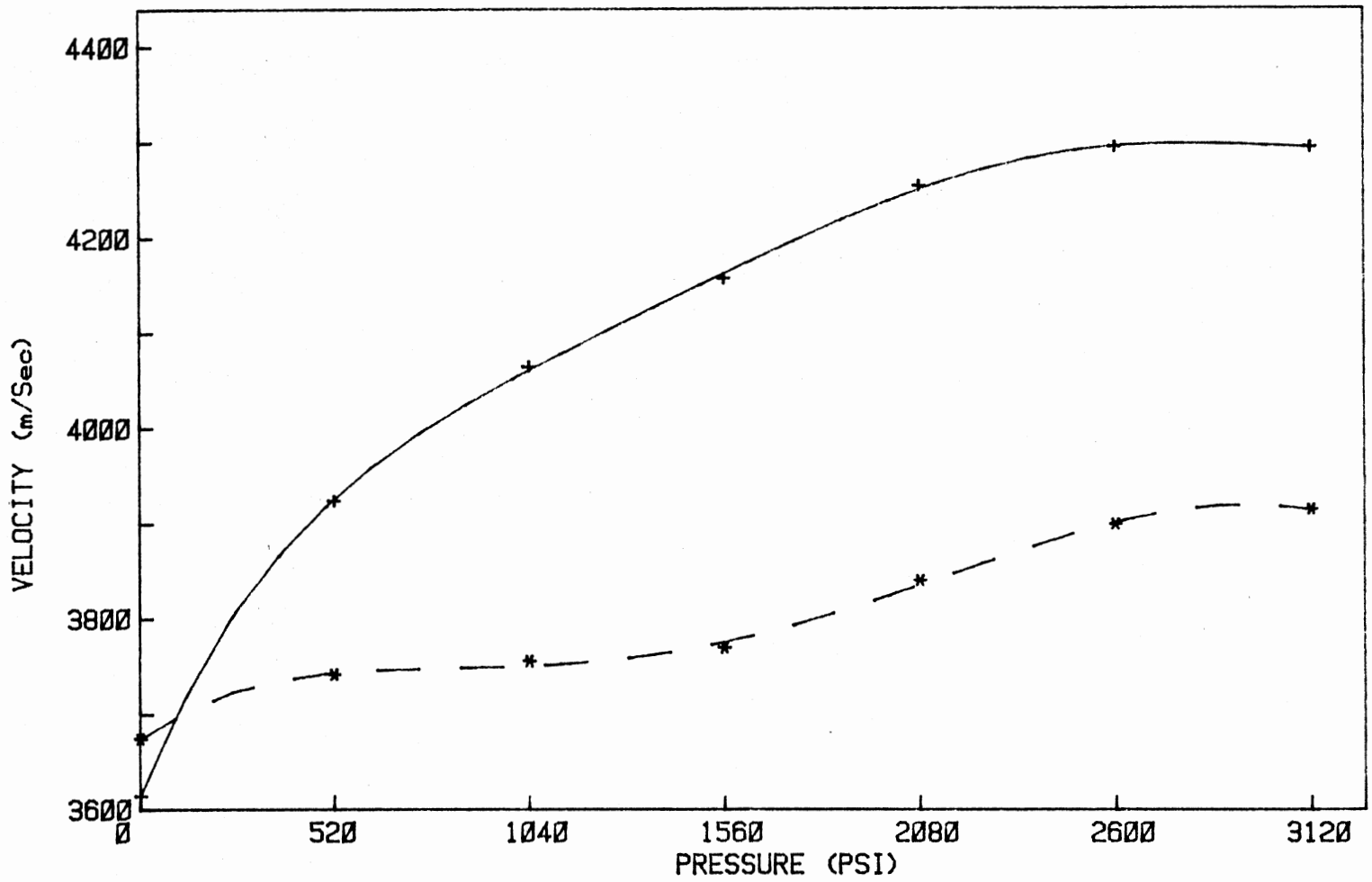

Figure 23. Velocity Verses Pressure For The Mesa Sandstone

TABLE III

ANALYSIS OF THE CHANGE IN VELOCITY WITH INCREASING PRESSURE FOR WATER SATURATED SANDSTONES

Calculated Variables	Sandstone Sample				
	1	2	4	Cockran	Mesa
Porosity	27%	23%	28%	7%	8%
Anisotropy Factor at:					
Zero Stress	1.01 (2%)	1.05 (5%)	1.05 (5%)	1.05 (5%)	1.02 (2%)
Maximum Stress	1.20 (18%)	1.12 (12%)	1.16 (15%)	1.17 (16%)	1.13 (12%)
Change in Velocity Parallel to the Applied Stress	20% (1.21)	24% (1.25)	18% (1.2)	20% (1.22)	17% (1.18)
Change in Velocity Perpendicular to Applied Stress	3% (1.03)	8% (1.08)	4% (1.07)	9% (1.1)	6% (1.03)

2. As the stress increases, both the velocity in the direction of the applied stress (perpendicular to the bedding planes), and the velocity perpendicular to the direction of the applied stress (parallel to the bedding planes) increase. This increase, for both velocities, has the biggest jump at low stress values and starts approaching a final stable value at higher stress values.

3. The increase in the uniaxial stress causes the velocity in the direction of the applied stress to increase at a higher rate than the velocity perpendicualr to this direction.

4. The unequal increase in both velocities causes the anisotropy factor to increase with increasing pressure values. This can be seen from the difference between the anisotropy factor values, at zero stress and at the maximum applied stress. Thus, the uniaxial stress, or unequal preloading, causes the samples to respond more anisotropically.

The change in velocity with the applied stress is due to the closing of cracks in each sample. These cracks are thought of as being randomly distributed over each sample. When the stress is applied in a certain direction, most of the cracks perpendicular to that direction close. This leads to an appreciable increase in that direction's velocity. Meanwhile, the cracks in the opposite direction (perpendicular to the stress) do not close completely, this leads to lower increase in that direction's velocity (as compared to the velocity in the direction of the applied pressure). To support this conclusion, cracks were generated in sandstone sample 1, by freezing the saturated sample in a refrigerator box for 48 hours. Figures 24 and 25 show the velocity in the direction of, and perpendicular to, the applied stress for sample 1, both before (solid curve) and after (dashed curve) the freezing of the sample. The

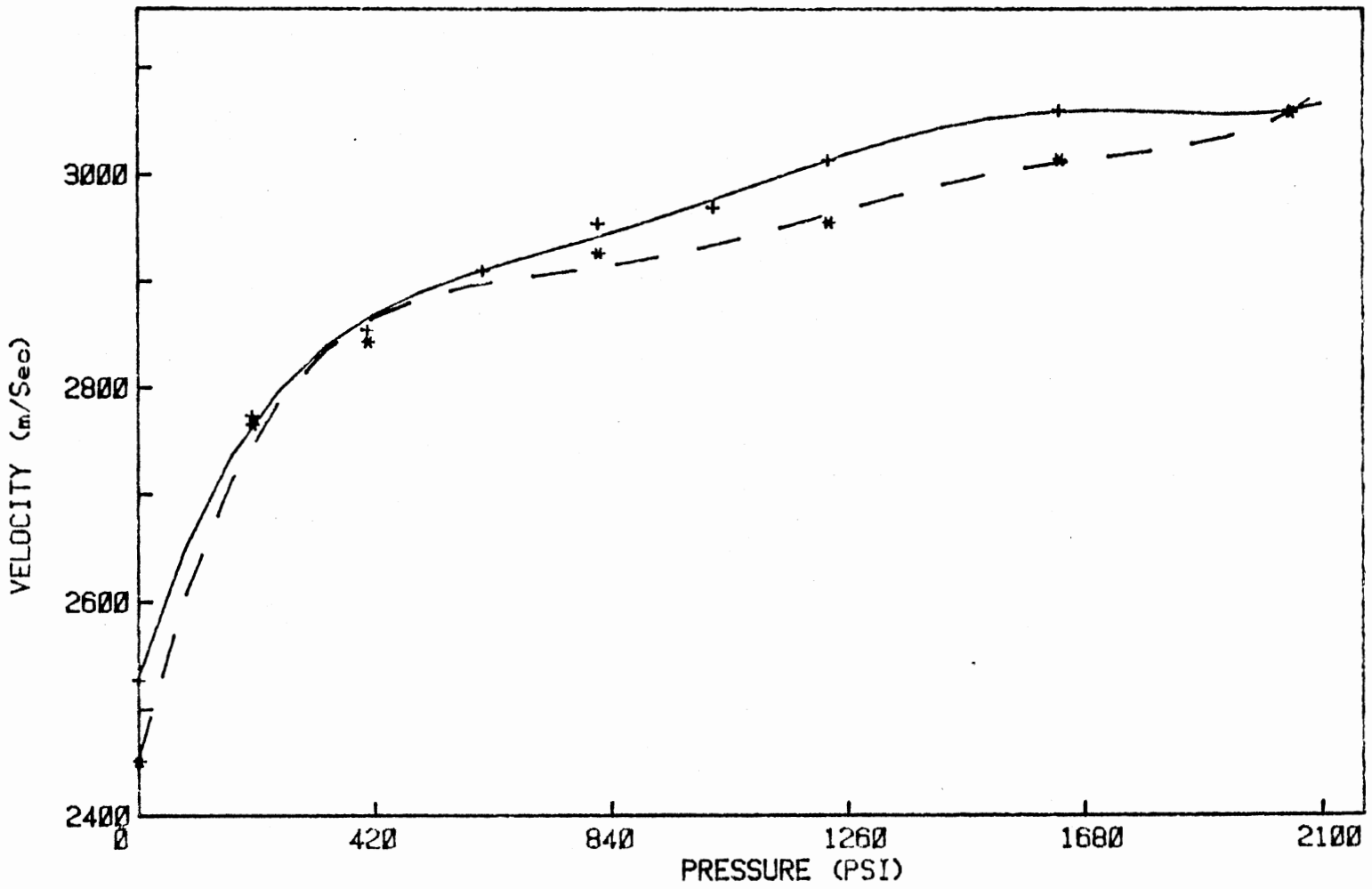

Figure 24. The Effect Of Microcracks On The Velocity Parallel To The Direction Of The Applied Stress For Sandstone Sample 1

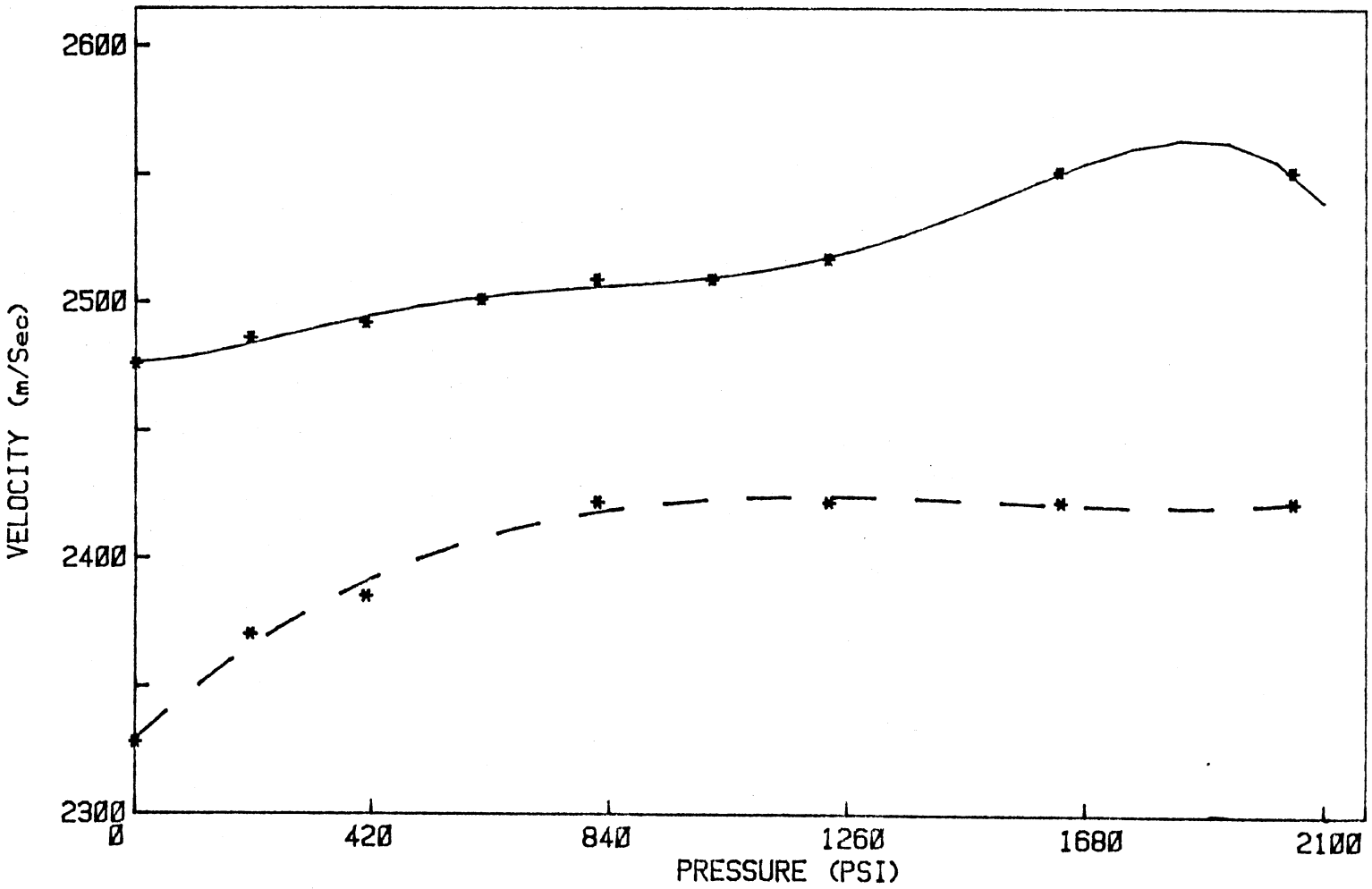

Figure 25. The Effect Of Microcracks On The Velocity Perpendicular To The Direction Of Applied Stress For Sandstone Sample 1

applied stress was perpendicular to the bedding planes. From Figure 24, the velocity at zero stress decreased by 3% after the freezing process. This percent difference between the velocities decreased to fall within the experimental error as the applied stress increased. In Figure 25, the velocity (perpendicular to the direction of the applied pressure) decreased by 6% at zero pressure, then as the pressure increased this percent difference decreased to about 4%.

Cracks were also generated in the Mesa sample by placing the saturated sample in liquid nitrogen. The velocities in the direction of the applied pressure are shown in Figure 26, where the solid curve represents measurements made before the freezing process, and the dashed curve stands for those measurements made after the sample was frozen. After the freezing process, this sample's velocity decreased by 6% at zero stress value and as the applied stress increased this percent difference decreased to about 5%, at intermediate pressures, then to 1.5% at the maximum applied stress.

The above analysis supports strongly the hypothesis that the random distribution of cracks effects the seismic velocity in sandstone samples.

The anisotropy in velocity also changes after the introduction of cracks in each sample. After the freezing process, the anisotropy factor for sample 1 increased to 1.05 (5%) at zero stress value. This corresponds to an increase of 3% from the value found before freezing this sample. Similarly, at the maximum applied stress, the anisotropy factor increased to 1.26 (23%). An increase of 5% as compared to the measurement found in Table III.

When the direction of stress was changed so that it is parallel to the bedding planes (Figure 27), the velocity in the direction of the

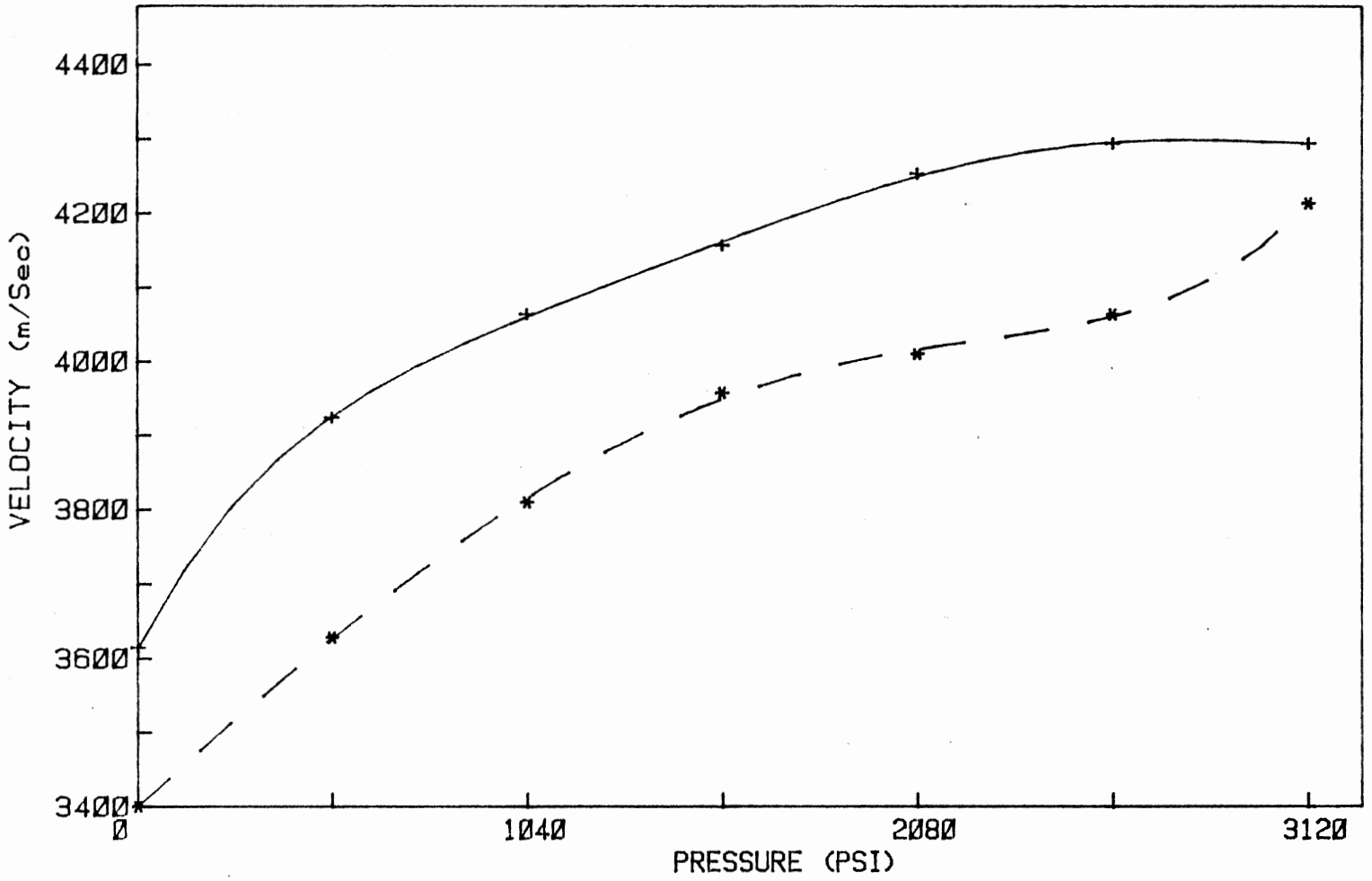

Figure 26. The Effect Of Cracks On The Velocity In The Direction Of The Applied Stress For The Mesa Sandstone

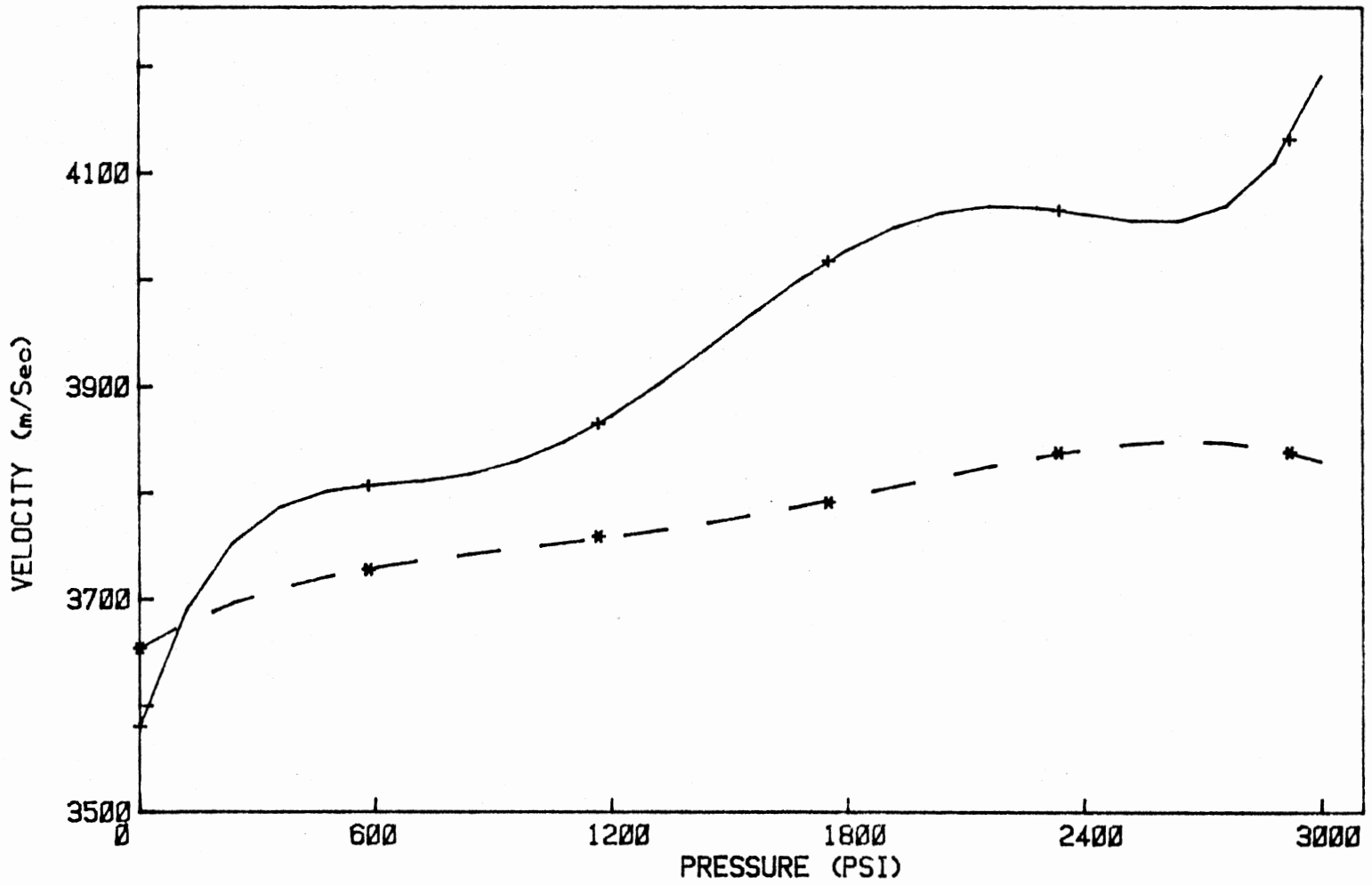

Figure 27. Velocity Verses Applied Stress For The Mesa Sandstone Sample, The Applied Stress Is Paralled To The Bedding Planes

stress was higher than when perpendicular to the stress although the magnitudes of the velocities are not the same as the previous measuring sequence (Figure 23). These measurements demonstrate that the cracks yield an anisotropic contribution to the stiffness. The closure of cracks which are aligned perpendicular to the stress leads to an increase in stiffness along the stress direction but not perpendicular to it. This component of the elastic properties then models the stress distribution in the samples. If the stress distribution is anisotropic, then the velocity distribution will reflect this anisotropy.

CHAPTER V

SUMMARY AND FUTURE SUGGESTIONS

In this study, some of the acoustic properties of sandstone were investigated. The samples used in this experiment contained very small amounts of clay, were quartz rich, well sorted and fine grained. The porosities of these samples were found to vary from 7% to about 30%. This wide range of porosities made the velocities (in saturated samples) vary from 2000 m/sec to about 4500 m/sec, with the low porosity samples having the higher velocities.

This study has also shown that seismic velocities in sandstone are independent of the frequency of the incident seismic pulse. This suggests that the frequencies used in the exploration work do not effect the time of flight of the seismic pulses in sandstone sedimentary rocks.

Next, it was found that the P-wave velocities in the direction paralleled to the sample's bedding planes were different from the velocities perpendicular to the bedding planes (anisotropy in the samples' velocities). The percent difference between these velocities (or anisotropy factor) increased as the uniaxial stress increased. Furthermore, the anisotropy factor was smaller when the applied stress was parallel to the bedding planes, than when it was perpendicular to the bedding planes, as can be seen from Figures 27 and 23. However, this last point should be investigated more by freezing the sample and carrying the velocity measurements with one combination of pressure-

bedding planes, then refreezing the sample and going through the same measurements with the other pressure-bedding planes combination. Such an experiment will also help in understanding more about the generation and preferred orientation of micro-cracks in sandstone. This will be done by comparing the velocities in the direction of the applied stress, when the stress is perpendicular to the bedding planes, to the velocities when the stress is paralleled to the bedding planes.

This experiment also showed that propagation perpendicular to the stress does not sample the same distribution of cracks as propagation parallel to the stress. The uniaxial stress closes cracks which are oriented perpendicular to the stress direction. Cracks oriented parallel to the stress direction are not closed and P-wave velocity in that direction does not change appreciably with pressure. Thus the symmetry of the stress defines a velocity anisotropy in the sandstone which depends on the directions and magnitude of the stress.

For future work the effects of microcracks on the velocities, the stiffness and the anisotropy of sandstone samples should be investigated in more details. Similarly, the same analysis should be carried on dry samples and compared to the results found above and to samples having different saturation levels.

BIBLIOGRAPHY

(1) Biot, M. A. "Theory of Propagation of Elastic Waves in a Fluid-Saturated Solid. I. Low-Frequency Range. II. Higher Frequency Range." The Journal of Acoustical Society of America, 28, 2 (March, 1956), pp. 179-189.

(2) Dobrin, Miston B. Introduction to Geophysical Prospecting. 3rd Ed. New York: McGraw Hill Book Co., Inc., 1952, pp. 2-54.

(3) Domenico, S. N. "Effect of Brine-Gas Mixture on Velocity in an Unconsolidated Sand Reservoir." Geophysics, 41, 5 (Oct. 1976), pp. 882-894.

(4) Geertsma, J., and D. C. Smit. "Some Aspects of Elastic Wave Propagation in Fluid-Saturated Porous Solids." Geophysics, 26, 2 (April, 1961), pp. 169-181.

(5) Gregory, A. R. "Fluid Saturation Effects on Dynamic Elastic Properties of Sedimentary Rocks." Geophysics, 41, 5 (Oct. 1976), pp. 895-921.

(6) Gregory, A. R., M. R. J. Wyllie, G. H. F. Gardner. "An Experimental Investigation of Factors Affecting Elastic Wave Velocities in Porous Media." Geophysics, 23, 3 (July, 1958), pp. 459-493.

(7) Hicks, W. G., and J. E. Berry. "Application of Continuous Velocity Logs to Determination of Fluid Saturation of Reservoir Rocks." Geophysics, 21, pp. 739-754.

(8) King, M. S. "Wave Velocities in Rocks as a Function of Changes in Overburden Pressure and Pore Fluid Saturants." Geophysics, 31, 1 (Feb., 1966), pp. 50-73.

(9) Levin, F. K. "The Reflection, Refraction, and Diffraction of Waves in Media With an Elliptical Velocity Dependence." Geophysics, 43, 3 (April, 1978), pp. 528-537.

(10) Postman, G. W. "Wave Propagation in a Stratified Medium." Geophysics, 20, 4 (Oct., 1955), pp. 780-806.

(11) Robinson, Enders A. and Sven Treitel. Geophysical Signal Analysis. New Jersey: Prentice-Hall, Inc., 1980, pp. 1-10.

(12) Shelton, J. W., Roy H. Bingham and William A. Jenkins. Geology and Mineral Resources of Noble County, Oklahoma. Oklahoma Geological Survey, Bulletin 128, The University of Oklahoma, Norman, 1979.

(13) Temkin, Samuel. Elements of Acoustics. New York: John Wiley and Sons, 1981.

(14) Toksoz, M. N., C. H. Cheng, and A. Timur. "Velocities of Seismic Waves in Porous Rocks." Geophysics, 41, 2 (Feb., 1976), pp. 621-640.

(15) Uhrig, L. F., and F. A. Van Melle. "Velocity Anisotropy in Stratified Media." Geophysics, 20, 4 (Oct., 1955), pp. 774-779.

(16) White, J. E. "Computed Waveforms in Transversely Isotropic Media." Geophysics, 47, 5 (May, 1982), pp. 771-783.

(17) White, J. E., S. N. Heaps, and P. L. Lawrence. "Seismic Waves From a Horizontal Force." Geophysics, 21, 3 (July, 1956), pp. 715-723.

(18) Wilson, M. B. and E. D. Pittman. "Authigenic Clays in Sandstones: Recognition and Influence on Reservoir Properties and Paleoenvironmental Analysis." Journal of Sedimentary Petrology, 47, 1 (Mar., 1977), pp. 3-31.

(19) Wyllie, M. R. J., A. R. Gregory, and L. W. Gardner. "Elastic Wave Velocities in Heterogeneous and Porous Media." Geophysics, 21, 1 (Jan., 1956), pp. 41-70.

VITA

Khalid Loudiyi

Candidate for the Degree of

Master of Science

Thesis: ACOUSTIC PROPERTIES OF SANDSTONE

Major Field: Physics

Biographical:

Personal Data: Born in Kenitra, Morocco, January 5, 1956.

Education: Graduated from Kenitra American High School, Kenitra, Morocco, in June, 1975; received the Bachelor of Science degree in Engineering Physics (Electronics) and Mathematics from Southwest Missouri State University, Springfield, Missouri, in May, 1980; completed the requirements for the Master of Science degree at Oklahoma State University in May, 1983.

Professional Experience: Undergraduate Laboratory Teaching Assistant, Southwest Missouri State University, 1979-1980; Graduate Teaching Assistant, Department of Physics, Oklahoma State University, 1980-1981; Graduate Research Assistant, Department of Physics, Oklahoma State University, 1981-1983.